

Review

Recent Advances of Nanostructured Materials for Photoelectrochemical Bioanalysis

Ling Zhang¹, Yuan-Cheng Zhu^{2,*}  and Wei-Wei Zhao³

¹ School of Electronic and Information Engineering, Jinling Institute of Technology, Nanjing 211169, China; zhangling@jit.edu.cn

² State Key Laboratory of Pharmaceutical Biotechnology, School of Life Science, Nanjing University, Nanjing 210023, China

³ State Key Laboratory of Analytical Chemistry for Life Science, School of Chemistry and Chemical Engineering, Nanjing University, Nanjing 210023, China; zww@nju.edu.cn

* Correspondence: yczhu@nju.edu.cn

Abstract: Nowadays, the emerging photoelectrochemical (PEC) bioanalysis has drawn intensive interest due to its numerous merits. As one of its core elements, functional nanostructured materials play a crucial role during the construction of PEC biosensors, which can not only be employed as transducers but also act as signal probes. Although both chemical composition and morphology control of nanostructured materials contribute to the excellent analytical performance of PEC bioassay, surveys addressing nanostructures with different dimensionality have rarely been reported. In this review, according to classification based on dimensionality, zero-dimensional, one-dimensional, two-dimensional, and three-dimensional nanostructures used in PEC bioanalysis are evaluated, with an emphasis on the effect of morphology on the detection performances. Furthermore, using the illustration of recent works, related novel PEC biosensing patterns with promising applications are also discussed. Finally, the current challenges and some future perspectives in this field are addressed based on our opinions.

Keywords: photoelectrochemical; biosensor; nanostructured materials; biosensing patterns; review



Citation: Zhang, L.; Zhu, Y.-C.; Zhao, W.-W. Recent Advances of Nanostructured Materials for Photoelectrochemical Bioanalysis.

Chemosensors **2022**, *10*, 14.

<https://doi.org/10.3390/chemosensors10010014>

chemosensors10010014

Academic Editor: Ali Othman

Received: 15 November 2021

Accepted: 27 December 2021

Published: 30 December 2021

Publisher's Note: MDPI stays neutral with regard to jurisdictional claims in published maps and institutional affiliations.



Copyright: © 2021 by the authors. Licensee MDPI, Basel, Switzerland. This article is an open access article distributed under the terms and conditions of the Creative Commons Attribution (CC BY) license (<https://creativecommons.org/licenses/by/4.0/>).

1. Introduction

Photoelectrochemical (PEC) phenomena have drawn intensive interest in many fields since being discovered by Becquerel in 1839 [1–3]. The PEC process typically refers to the conversion of light energy to electrical power due to the light absorption-induced excitation and transport of electrons. As an emerging sensing technology, PEC bioanalysis integrates the PEC process and electrochemical biosensing delicately. As shown in Figure 1, a typical PEC analysis system usually includes three parts: a light-source system, detection system, and signal-reading system. As the core part, the detection system is generally composed of three electrodes and an electrolyte. Therefore, photoactive species-modified working electrodes play an important role in the construction of PEC sensors. Taking commonly used semiconductor nanoparticles (NPs), for example, under illumination, photoactive species generate electron–hole (e–h) pairs through the excitation of photoelectrons from the valence band (VB) to the conduction band (CB). With the neutralization of holes by donors (D) or the capture of electrons by acceptors (A) on the interface of working electrodes, constant and stable anodic or cathodic photocurrent signals can be achieved from the transport of electrons. Once the targets trigger specific biorecognition events alter the abovementioned PEC process, the photocurrent signals change. By monitoring the chronoamperometric *I*–*t* responses with a signal-reading system that reflects the concentration variation of target analytes, the biochemical analytes of interest can be detected. Compared with traditional electrochemical bioanalysis, PEC bioassay perceives higher sensitivity due to its significantly improved ratio of signal to noise ascribed to the fact that the excitation source and the

detection signal have different energy forms. Moreover, the merits of low cost, convenient operation, and easy miniaturization further accelerate the boom of PEC analysis.

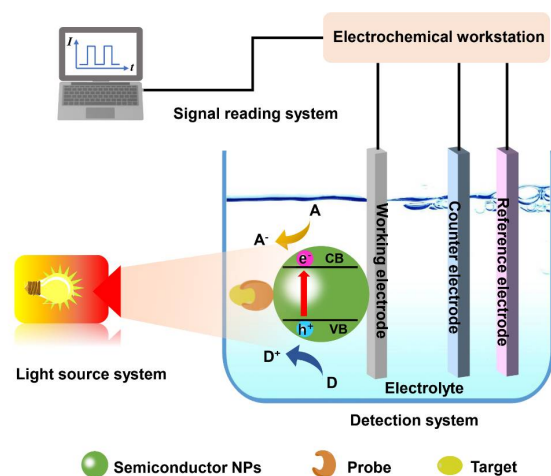


Figure 1. Diagram of typical PEC biosensing system.

As above, the exploitation of photoactive materials with proper structures and high photoelectrical conversion efficiencies will be crucial to the improvement of PEC biosensing performances. For PEC biosensors, the commonly used photoactive materials are nanostructured semiconductors. Through the optimization in size, porosity, morphology, and the functional groups, nanostructured materials can acquire more excellent biosensing properties. Recently, according to the differences in chemical compositions, various photoactive materials used in PEC bioassays have been summarized in many reviews [4–7]. However, few surveys addressing different types of nanostructures employed for PEC sensing applications have been systematically conducted.

In view of the advances in PEC bioassays over the past five years, this review attempts to systematically summarize the functional nanostructured materials used in PEC biosensing from the prospect of dimensionality and highlights several novel PEC biosensing patterns that have promising practical application prospects, with illustrated examples.

2. Functional Nanostructure-Based PEC Biosensing

Nanostructured materials typically refer to low-dimensional materials with a sub-micron or nanoscale size of structural units in at least one direction [6,8]. In order to enhance the PEC biosensing performance, many functional nanostructured materials have been developed to serve as transducers, probes, and carriers due to their numerous unique properties. Except for the chemical component, rational morphology regulating of nanostructure surfaces can effectively increase their active sites and improve their target-capture ability. Therefore, extensive efforts have been devoted to the morphology control of functional nanostructures. Classified by dimensionality, nanostructures include zero-dimensional (0D), one-dimensional (1D), two-dimensional (2D), and three-dimensional (3D) structures [8] that exhibit a profound impact on PEC biosensing performance. In this section, various functional nanostructured materials with different dimensionality used for high-performance PEC bioanalysis are discussed.

2.1. 0D-Nanostructure Materials

Over the past several decades, 0D-nanostructure materials, with no dimension greater than 100 nm, have been widely used in the construction of sensitive PEC biosensors. As the simplest nanostructure, 0D nanostructures typically include the most commonly used quantum dots (QDs) and nanoparticles (NPs). Herein, the PEC sensing performance using QDs, carbon-based NPs, and metal-based NPs as functional nanostructured materials is discussed.

2.1.1. QDs

QDs, discovered in the 1980s [9,10], have boomed in many biosensing fields such as optics, electronics, catalysis, and so on by coupling with various biomolecules. In the early 2000s, a QD–biomolecule nanohybrid was first applied to PEC analysis [11], which subsequently stimulated substantial interest in experimental and theoretical research in the field of QD-based PEC biosensing. The tailored physicochemical property is one of the most attractive reasons for favoring QDs in PEC biosensing. For example, different from bulk materials, the bandgaps of QDs can be easily regulated by manipulating their size and composition [12–15]. Besides, compared to many other photoactive materials, QDs are easier to synthesize and surface-modified. Their photoelectric conversion activity and chemical stability are fantastic as well. Additionally, with the comparable size to biomolecules and the multifunctional group-modified interface, it is very easy for QDs to construct various kinds of architectures for advanced PEC biosensing platforms.

As photoactive materials, under illumination, semiconductor QDs can generate stable anode or cathode current signals in the presence of suitable electron donors or electron acceptors. Based on this, numerous semiconductor QD-modified electrodes have been developed for the construction of elegant PEC sensing architectures. Compared to “signal on” PEC analysis, “signal off” PEC sensing patterns often have unsatisfied sensitivity due to the limited background signal of photoactive materials. Addressing this challenge, Zhang et al. reported that a PEC assay of CA125 based on the core-shell nanostructure of SiO₂@polydopamine (PDA) served as a quencher to CdTe QD-modified ITO. The high photoelectric activity of CdTe QDs coupled with the highly efficient signal quencher contributed to the ultra-low detection limit of 0.3 U L⁻¹ [16]. The combination of two or more semiconductor QDs with matching bandgaps is a good way to enhance their ability to absorb visible light and improve the efficiency of charge separation and charge transfer, as well. For example, by using low-bandgap Ag₂S QDs as the photosensitizer, the photocurrent intensity of a ZnS@Ag₂S QD-modified electrode improved 10 and 1.4 times more than that of ZnS QDs and Ag₂S QDs, respectively. From this, based on Hg²⁺ triggered the formation of HgS/ZnS@Ag₂S, Wang et al. proposed a “signal on” PEC sensor for the assay of Hg²⁺, which had the detection limit of 1.0 pM [17].

As mentioned above, in PEC assays, photoactive materials are often directly modified on the sensing interface, which could affect the sensitivity and detection limit during the sensing process due to the high initial photocurrent signal and the un neglected background noise. Faced with this issue, Yuan et al. proposed a near-zero background noise PEC biosensor for the detection of microRNA-141. As seen in Figure 2a, the CdTe QDs-methylene blue (MB)-modified DNA tetrahedron (TET) was brought in close proximity to the surface of a cDNA-anchored golden NP (Au NP) immobilized glassy carbon electrode (GCE) by the target DNA (tDNA)-controlled hybridization of cDNA, output DNA, and DNA TET-CdTe QDs-MB complex. Due to the outstanding photovoltaic performance of the TET-QD-MB complex coupled with the enzyme-assisted target-cycling amplification strategy, the proposed PEC biosensor possessed a low detection limit of 17 aM for the detection of miRNR-141 [18].

Despite the superior PEC response, inorganic semiconductor QDs still suffered from several hurdles during the PEC analysis. For example, the widely used inorganic QD Cd-chalcogenide had a potential risk of metal ion leakage, such as Cd and Se, which might influence its application in vivo analysis. In view of the above problem, our group fabricated a tetraphenylporphyrin (TPP)-doped poly[(9,9-dioctylfluorenyl-2,7-diyl)-co-(1,4-benzo-[2,1',3]-thiadazole)] (PEBT) polymer dot (Pdot)-modified ITO electrode. By choosing L-cysteine as the PEC detection model molecule, we found that this TPP-doped PFBT Pdot shows excellent photostability and biocompatibility. In this work, the PEC biosensing performance of the TPP-doped PFBT Pdot was demonstrated in detail for the first time [19]. After that, our group reported a series of works based on Pdots [20–24]. For instance, using the energy transfer (ET) process between the Pdots and Au NPs, a “signal on” PEC biosensing platform was constructed by us to probe the telomerase activity in cell

extracts [23]. Besides, we also originally fabricated the heterojunction of semiconducting Cd-chalcogenide QDs and Pdots, and the corresponding PEC assay property for the detection of L-cysteine was evaluated [24].

2.1.2. Carbon-Based NPs

Carbon is one of the most substantial elements in both organic and inorganic materials. In recent years, carbon-based nanostructured materials have attracted increasing research interests in the PEC biosensing field due to their unique physicochemical and electronic characteristics [25–30]. Of the various carbon-based nanostructured materials, such as graphene, fullerene C₆₀, and g-C₃N₄, only 0D nanostructures will be presented in this part.

Compared to other metallic-based NPs or organic photosensitizers, carbon nanodots (C-dots) are widely used in bioimaging [31–33] and biosensing areas [34–36] because of their low cytotoxicity, resistance to photobleaching, and fascinating biocompatibility [37]. For example, Yu et al. reported on an N-doped C-dot-immobilized TiO₂-Pt NP-modified paper-based PEC sensor for the detection of carcinoembryonic antigen (CEA) in human serum. Benefiting from this fabricated hierarchical nanostructure, the significantly enhanced conductivity and the greatly widened visible light absorption range were acquired by the prepared photoelectrode. In addition, though incubation with MCF-7 cells, the cytotoxicity test demonstrated that this C-dot-based nanomaterial had low toxicity to live cells [38]. Using boronic acid-modified C-dots (B-CDs) as the signal probe, Yin et al. proposed that a “signal on” multifunctional PEC biosensor for the assay of 5hmC or β-GT based on the T4-β-glucosyltransferase (β-GT) triggered the glycosylation of 5hmC, which brought a B-CD probe to the surface of a WS₂ nanosheet-fabricated ITO electrode and led to an increase in photocurrent responses [39].

As a metal-free semiconductor, nitrogen graphene quantum dots (NGQDs) have drawn special attention in various PEC applications due to their size-dependent and edge-sensitive photoluminescence characteristics [40–42]. For instance, Wang et al. found that, loaded with the right amount of NGQDs, the photogenerated charge carriers of semiconductor nanomaterials would get extended lifetimes. In this ground, they fabricated NGQD-modified MoS₂ nano hybrids used for label-free PEC aptasensing [43]. Instead of being immobilized on the electrode surface, QDs can also be treated as signal probes by labeling various biomolecules. As shown in Figure 2b, the PEC performance of the ZnO/CdTe QD nano hybrid was improved significantly by the local surface plasmon resonance resulting from the nanogold-assembled mesoporous silica NPs (GMSNs). Subsequently, the N-glycan expression on the cell surface was evaluated by the immobilization of concanavalin A-conjugated GQD (GOD@Con-A) near the as-prepared photoelectrode's surface based on the Con A-triggered specific recognition with target cells. With horseradish peroxidase (HRP) labeled on multiple branched-arm double-helix DNA (HRP-mdhDNA), a luminol-based chemiluminescent (CL) system was used as the inner light source for the sensitive sensing of N-glycan expression on the target cell surface [44].

Compared with 2D bulk g-C₃N₄, the g-C₃N₄ QDs with unique quantum size achieve more active sites and enhanced visible light absorption ability [45]. Specially, the hybridization of g-C₃N₄ with other nano semiconductors with suitable bandgaps could further accelerate the electron transfer and inhibit the recombination of charge carriers. Using g-C₃N₄ as the sensitizer, Tan et al. constructed a PEC biosensor for the assay of a CCRF-CEM cell by employing g-C₃N₄-combined ZnO nanodisks (ZnO NDs@g-C₃N₄) as the photoactive material. The interfacial built-in fields of the as-prepared heterojunction had consistent direction with the diffusion path of minority charge, which significantly increased the separation of photon-induced electron–hole pairs instead of their recombination, and the detection limit was calculated to be 20 cell/mL [46].

2.1.3. Noble-Metal NPs

Owing to their fantastic optical and electrical properties, noble-metal NPs have attracted great interest in nanostructure-based PEC analysis. Among various noble-metal

NPs, Au NPs and Ag NPs are the most relevant in bioanalysis because they are easy to prepare in different sizes and have excellent stability and biological compatibility.

Addressing to improve the visible light-harvesting and photoelectric conversion ability, noble metal NPs, such as Au NPs, Ag NPs, or a combination of both, are often used for the modification of various semiconductors due to their surface plasmon resonance (SPR) effects. Under illumination, hot electrons would generate from the oscillation of conduction electrons at the surface of plasmonic metal nanomaterials. Due to the higher energy, these hot electrons would easily inject the semiconductors with the matched bandgap. By further transferring to the external circuit, an enhanced photocurrent signal would be obtained. In addition, the density of carriers and the intensity of the photocurrent could also be improved by transferring energy from plasmonic metal NPs to semiconductors [47]. Therefore, based on the SPR effect, numerous PEC bioassay methods have been reported in recent years [48]. For instance, Zhang et al. developed a PEC analysis for M.SssI methyltransferase (M.SssI MTase) through target-triggered photocurrent enhancement resulting from the Au NP-mediated SPR effect. The significant increment of the photocurrent was mainly ascribed to the fantastic conductivity and SPR effect of Au NPs coupled with the sensitization of rhodamine (RhB) [49]. Ding et al. studied the PEC property of Au nanoclusters (Au NCs) effected by the Ag NP-based SPR. As displayed in Figure 2c, an Au NC-decorated Ag@SiO₂-modified FTO photoelectrode (Au NC-Ag@SiO₂/FTO) was fabricated. By adjusting the distance between the Au NCs and Ag NPs by changing the thickness of the silica shell, the photocurrent intensity of the fabricated Au NC-Ag@SiO₂/FTO electrode increased to 3.8 times higher than that of the Au NC-modified FTO photoelectrode, which might be attributable to the synergistic effect of hot electron transfer, light-scattering effects, and energy transfer [50]. With regard to the application of SPR in PEC biosensing, our group has a series of reports, as well [51–53]. For example, to improve the visible light-harvesting property of TiO₂ nanorod-modified FTO electrodes, further decoration with Au@Ag NPs was employed. Thanks to the excellent SPR effect of the Au@Ag nanohybrid, threefold enhancement of the photocurrent intensity was acquired [52].

Noble-metal NPs with an SPR effect have also been demonstrated to be powerful nanoprobes of PEC biosensing applications based on the interparticle resonance energy transfer (RET) between energy-donor semiconductors and plasmonic noble-metal NPs. When the SPR absorption spectrum of plasmonic NPs has a large overlap with the emission spectrum of semiconductors, the RET takes place, which accelerates the recombination of photogenerated electrode–hole pairs and quenches the photocurrents. Incidentally, the distance from energy donor to energy acceptor is another critical factor to improve the quenching efficiency of photocurrents [54]. Attracted by the high sensitivity of the RET strategy, many noble-metal NP-based nanoprobes have recently been developed to translate the biomolecular recognition process to the change of photocurrent signals. For example, based on the RET between Ce-TiO₂@MoSe₂ and Au NPs, Liu et al. proposed a “signal on” PEC aptasensor for highly sensitive sensing of AFB1 [55]. Also using Au NPs as the energy acceptor, our group realized the ultrasensitive PEC detection of miRNA-141 by coupling an entropy-driven toehold-mediated DNA strand displacement (ETSD) reaction with an RET signal strategy [21]. Another interesting example is that the RET process of oligonucleotide-encapsulated Ag nanoclusters (Ag NCs) against CdS QDs was estimated, and by detecting the target-induced changes of photocurrent intensity, a DNA PEC sensor with a limit detection of 0.3 pM was developed by us [56]. After that, we synthesized the Ag@Au asymmetric core–satellite nanostructures (Ag@Au ACS), which were used to implement the PEC immunoassay of prostate-specific antigen (PSA) on the basis of the RET interaction between Ag@Au ACS and CdS QDs [57].

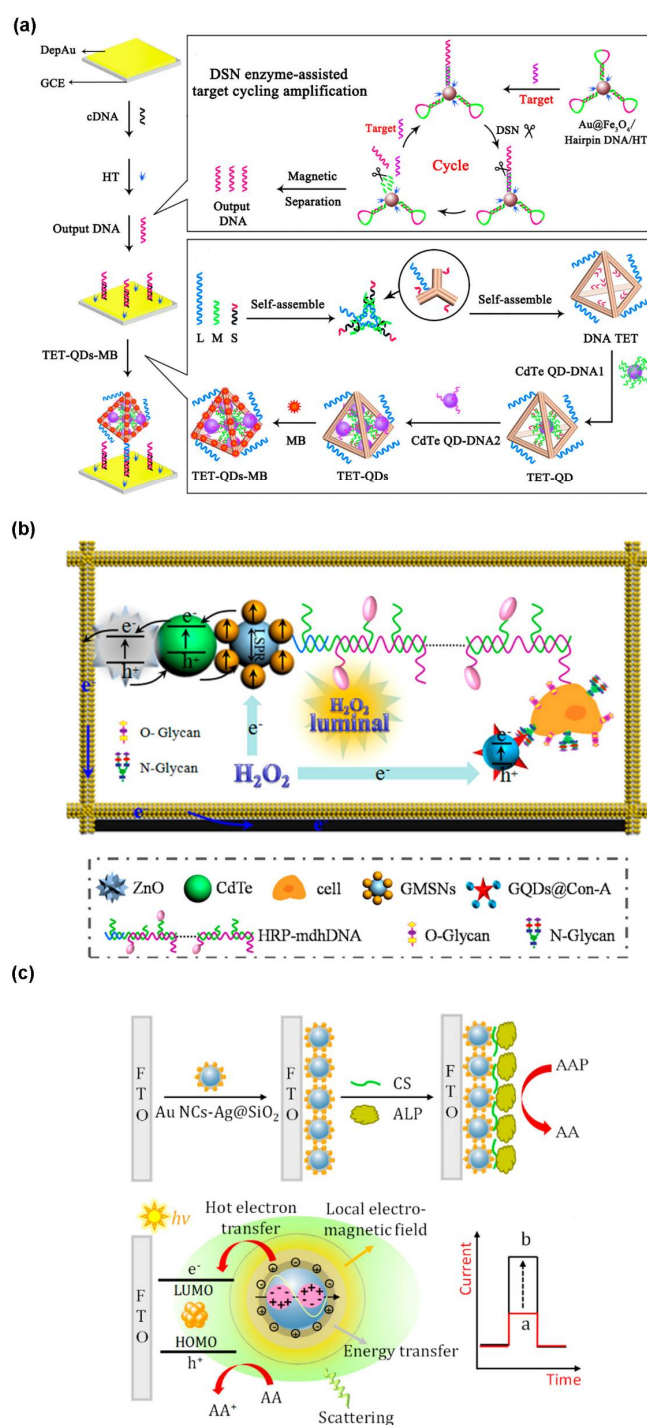


Figure 2. (a) Schematic diagrams of the PEC biosensor for miRNA-141 determination. Reprinted with permission from ref. [18]. Copyright 2018, American Chemical Society; (b) schematic representation of the PEC analytical principle for N-glycan expression. Reprinted with permission from ref. [44]. Copyright 2017, American Chemical Society; (c) the energy diagram of the SPR effect-induced photocurrent enhancement system. Reprinted with permission from ref. [50]. Copyright 2020, American Chemical Society.

2.2. 1D-Nanostructure Materials

1D nanostructures are typically defined as high-aspect-ratio nanomaterials with diameters ranging from 1 to 100 nm, such as the morphologies of nanorods, nanowires, nanotubes, nanobelts, nanoneedles, and so on [58]. Compared to bulk semiconductors, the

high surface-to-volume ratio significantly increases the binding sites for various surface reactions and greatly accelerate the transfer speed of photogenerated charge carriers from the interior to the surface of 1D nanomaterials. Besides, the quantum effects can expect to be modulated by adjusting the diameter of the 1D nanostructures [59]. For the past few years, these fascinating characteristics have attracted extensive concerns in PEC analysis applications [60–63]. Here, we will discuss the commonly used 1D nanomaterials in PEC bioanalysis according to the difference in chemical composition.

2.2.1. Metal Oxide-Based Semiconductors

Because of the strong light-absorption property, low toxicity, and high chemical stability and biocompatibility, metal oxide-based 1D nanomaterials such as TiO₂, ZnO, CuO, and Fe₂O₃ have broad application prospects in PEC transducing or signal probing, which are usually immobilized or grown in-situ on the surface of substrate materials.

Among various oxide nanostructures, different morphologies of TiO₂ nanostructures have attracted much attention [64–67]. Compared to NP-based PEC biosensors, TiO₂ nanowire (NW) structures can significantly reduce the transfer time of charge carriers from the interior to the surface due to the tiny radial transmission distance and provide a more favorable transfer route for charge carriers, which are beneficial for the efficient separation of photogenerated charge carriers [68,69]. Feng et al. proposed a triphase bio-photoelectrode (TBP) system for the PEC detection of glucose by immobilizing glucose oxidase on the surface of TiO₂ NWs grown in situ on a superhydrophobic carbon textile substrate. In Figure 3a, a solid–liquid–air triphase interface was presented on the surface of this fabricated nanowire array immobilized superhydrophobic substrate, which supplied oxygen for the enzymatic reaction with much higher transport efficiency than a solid–liquid diphasic interface. As a result, the biosensing performance was significantly improved. In addition, the photocurrent response properties of TiO₂ NWs and TiO₂ NPs were evaluated. The results demonstrate that the former electrode had higher sensitivity and a lower detection limit than the latter [70].

In order to improve the visible light absorption performance of metal oxide-based semiconductors without an input offset voltage, coupling them with a narrow bandgap of nanomaterials or sensitizers is the most commonly used and most efficient strategy. For instance, Wei et al. fabricated MoO₃-modified TiO₂ nanoneedle photoelectrodes with carbon cloth as the substrate. The well-matched alignment of the as-prepared nanocomposites efficiently depressed the recombination of photogenerated electron–hole pairs and a fourfold increase in photocurrent intensity was accomplished [71]. As for QD sensitization, based on the fact that carboxyl- and amino-modified CdTe QD-immobilized ZnO NRs could significantly accelerate the transport of photogenerated electrons, Yu et al. proposed a cascaded photoactive nanostructure that significantly improved the visible light absorption property and amplified photocurrent responses [72]. Zhang et al. developed a highly selective PEC sensor for lysozyme by using Au NP-decorated Fe₂O₃ NRs as photoactive electrodes. The high aspect ratio of the fabricated nanorod structure was beneficial to shortening the transport distance of the photogenerated electrodes. Meanwhile, the Au NPs on the surface of Fe₂O₃ NRs facilitated the depression of the recombination of charge carriers as well. As a result, the detection limit of lysozyme was shown to be 3 pM [73].

2.2.2. Metal Chalcogenide-Based Semiconductors

As narrow-bandgap semiconductors, CdS nanostructures with various morphologies have been fabricated for PEC biosensing [74,75]. Among them, 1D-structure CdS NRs have shown tremendous potential in PEC applications due to the significantly increased binding sites and the decreased radial transport distance [76]. For example, Lei et al. fabricated beta-cyclodextrin-modified CdS NRs (β-CD@CdS NRs), which were applied to detect human immunodeficiency virus (HIV) DNA based on a target triggered biocatalytic precipitation (BCP) signal strategy combined with catalytic hairpin assembly (CHA) for signal amplification. Due to the excellent photoelectricity property of CdS NRs and

the reliable biorecognition peculiarity of β -CD, the detection limit of the biosensor was calculated to be 1.16 fM [77]. Illuminated by the outstanding catalytic performance of single-atom metal materials [78,79], using CdS NRs decorated with platinum single atoms (Pt SAs/CdS) as the photosensitive material, Zhu et al. constructed an ultrasensitive PEC immunoassay system for PSA detection based on an ion-exchange reaction (Figure 3b). As shown, although the decoration of both Pt NPs and Pt SAs can significantly increase the photoconversion efficiency, the photocurrent intensity of Pt SA/CdS NR electrodes was almost twofold higher than that of Pt NPs/CdS NRs due to the increase in excited charge-carrying concentration of CdS NRs induced by Pt SAs [80].

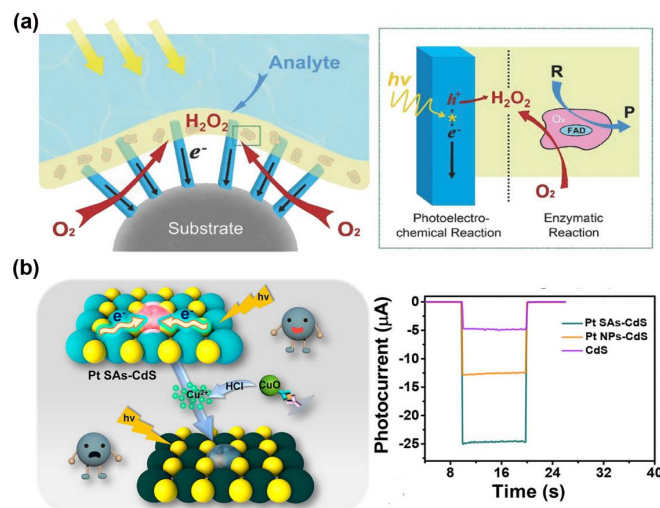


Figure 3. (a) Schematic illustration of the solid–liquid–air triphase bio-photoelectrode (TBP-electrode). Reprinted with permission from ref. [70]. Copyright 2018, John Wiley and Sons; (b) schematic illustration of the mechanism of Pt SA-CdS-based PEC biosensing platform and photocurrent responses for CdS, Pt SAs-CdS, and Pt NP-CdS. Reprinted with permission from ref. [80]. Copyright 2021, American Chemical Society.

Due to the notable near-IR and visible light-harvesting characteristic and the regulable bandgap, bismuth sulfide (Bi_2S_3) exhibits great potential in PEC bioanalysis applications [81,82]. For instance, Zhang et al. used Bi_2S_3 NRs as the photosensitive material to develop a “signal on” PEC sensing platform for the detection of polynucleotide kinase (PNK). Because of the high visible light absorption coefficient of Bi_2S_3 NRs and the dual-signal amplification strategy of steric hindrance coupled with nanozyme catalytic precipitation, the biosensor presented a low detection limit of $1.27 \times 10^{-5} \text{ U} \cdot \text{mL}^{-1}$ [83]. NW structures with very small diameters (typically smaller than Bohr radii) are often called ultrathin semiconductor nanowires (USNWs). Contrasted with regular NWs, USNWs demonstrated outstanding PEC performance due to their higher aspect ratio and quantum size effect. From this, Li et al. synthesized ZnSe USNWs with different diameters, and their size-controlled bandgaps and photoelectrical properties were evaluated [84].

2.2.3. Carbon Nanotube-Based Semiconductors

With the appearance of various allotropes of carbon, carbon nanomaterials have attracted close attention in many biosensing applications due to their special electronic structures and fascinating physicochemical properties. As one kind of promising 1D nanostructure, carbon nanotubes (CNTs) demonstrate excellent photogenerated electrons transfer property, which would significantly enhance the photocurrent signals of photoactive nanomaterials during PEC analysis.

For instance, Yang et al. fabricated a TiO_2 NP-coated multiwalled CNT nanohybrid on the substrate of FTO for the biosensing of microcystin-LR (MC-LR). The photocurrent of TiO_2 @CNT/FTO is about eight times than that of TiO_2 (P25)/FTO due to the notable

enhancement in conductivity of the core–shell nanostructure, and the sufficient covalent bonds induced electronic coupling and interaction on the nanohybrid interface [85]. Considering the fact that the heterojunction of an amine-modified MIL-68(In) coupled with CdS NPs could efficiently suppress the recombination of photogenerated electron–hole pairs and the multiwalled CNTs could dramatically enhance the photoelectric conversion properties by regulating the electrons transport paths, Yan et al. constructed a sensitive PEC aptamer biosensor for tetracycline (Tc) sensing by employing MIL-68(In)-NH₂/MWCNT/CdS/ITO as the photoactive electrode. Under the optimal condition, the photocurrent intensity of the fabricated MIL-68(In)-NH₂/MWCNT/CdS hybrid was improved to 7.8 times and 5.5 times higher than that of ITO/CdS and ITO/MIL-68(In)-NH₂/CdS, respectively. The detection limit of the proposed biosensor was calculated to be 0.015 nM [86]. In order to avoid the possible effect of the photoelectric conversion process on biological recognition events, Fan and Shi et al. constructed a double-electrode PEC carcinoembryonic antigen (CEA) bioassay platform with ZnIn₂S₄-immobilized Fe³⁺-doped TiO₂ NTs (ZIS/Fe:TiO₂ NTs) as the photoanode and Ag NP-decorated CNTs (Au/CNTs) as the cathode for biological recognition. The results demonstrate that the photogenerated electrons that came from the ZIS/Fe:TiO₂ NT photoanode were collected rapidly by the Au/CNT-anchored cathode due to the excellent electrical conductivity of Au NPs and CNTs, which greatly improved the sensitivity and selectivity of the developed PEC biosensor [87].

2.3. 2D-Nanostructure Materials

Since graphene sheets were successfully exfoliated from graphite in 2004 [88], 2D-nanostructure materials have attracted great concern in biosensing applications. 2D materials have many unique physicochemical properties, such as large surface area, abundant active sites, excellent electrical conductivity, tunable bandgap, and outstanding biocompatibility [89]. As a result, these nanostructures have exhibited promising prospects in the PEC bioassay field. Generally, the most commonly used 2D nanostructure for the construction of PEC detection platforms is nanosheets, which are a planar structure with a thickness of less than 100 nm. Except for graphene, other 2D nanosheets, such as graphene-like carbon nitride (g-C₃N₄), transition metal dichalcogenides, bismuth oxyhalides, 2D organic frameworks, MXenes (e.g., Ti₃C₂), and Xenes (e.g., black phosphorus), have enriched the family of photoelectrical nanomaterials. Given space limitations, only several typical types of 2D nanostructures will be introduced here.

2.3.1. Carbon-Based Graphene-like 2D Nanostructures

As the typical representative of 2D nanostructures, graphene has excellent electron-transport ability and satisfactory surface functionalization properties because of its outstanding electron conductivity and high specific surface area. Therefore, the sensitivity and selectivity of PEC bioanalysis are expected to be highly improved by the introduction of graphene nanomaterials. Because the bandgap of graphene is zero, this material is usually used to collect and transport electrons. Therefore, numerous graphene-based nanohybrids have been fabricated to improve their photoelectric conversion efficiency. For instance, contrasted with Mo-doped BiVO₄ (Mo-BiVO₄), the further incorporation of graphene achieved six times more enhancement in photocurrent signals, which demonstrates that graphene efficiently accelerated the transfer of electrons and facilitated the separation of photogenerated electrons and holes. In addition, the π – π stacking interaction of graphene also showed great potential in coupling with targets [90].

In order to improve the photoelectric conversion activity of graphene, heteroatom doping is another widely accepted way, by which the graphene adjusts its bandgap to improve its visible light-harvesting ability. In particular, boron (B) and nitrogen (N) are the most reported dopants because both of them have similar electronegativity to C, which makes graphene exhibit a special electronic structure. From this, Wang fabricated a high-performance photoactive electrode by attaching Bi₂MoO₆ to the N and B co-doped graphene (BNG). Due to the synergy of oxygen vacancy generated from the reduction of Bi₂MoO₆

and BNG in contrast with Bi_2MoO_6 , $\text{Bi}_2\text{MoO}_6/\text{graphene}$, $\text{Bi}_2\text{MoO}_6/\text{N-doped graphene}$ and $\text{Bi}_2\text{MoO}_6/\text{B-doped graphene}$, the $\text{Bi}_2\text{MoO}_6/\text{BNG}$ exhibited increases of about elevenfold, sevenfold, threefold, and twofold in photocurrent intensities, respectively [91].

Aside from doping heteroatom-doped graphene, graphene oxide (GO) fabricated from the oxidation of graphite has also received growing interest in PEC analysis due to its abundant active sites, aqueous dispersity, and narrow bandgap [92]. For example, Lin et al. fabricated a photoactive electrode with excellent PEC performance by coupling a porphyrinic metal–organic framework with reduced graphene oxide (PCN-224/rGO), which was used to detect p-arsanilic acid (p-ASA) depending on the strong affinity between the target and the as-prepared transducer. Because the recombination of photogenerated charge carriers was inhibited efficiently, the sensitivity of the biosensor was significantly improved and a detection limit of $5.47 \text{ ng}\cdot\text{L}^{-1}$ was obtained [93]. Apart from being used as transducers, GO can also be treated as a nanoprobe [94]. As shown in Figure 4a, considering the attractive PEC performance of alkylated C_{60} (AC_{60}), the excellent electronic conductivity of graphite flakes (Gr), and the abundant carboxyl active sites of GO, Zhang et al. fabricated a photoactive nanohybrid of $\text{AC}_{60}\text{-Gr-GO}$. Under illumination with visible light, the photocurrent signal of $\text{AC}_{60}\text{-Gr-GO}$ was 35 times higher than that of AC_{60} , whereafter, using the as-prepared $\text{AC}_{60}\text{-Gr-GO}$ as the labeled conjugate, a high-performance immunosensor for alpha-fetoprotein (AFP) was developed [95].

As the most stable allotrope of carbon nitride polymer, $g\text{-C}_3\text{N}_4$ constructed from the sp^2 hybridization of carbon atoms possesses a similar layer structure as graphene and metal-free covalent semiconductor properties [96]. Due to the comparatively small bandgap of 2.7 eV, easy fabrication, low toxicity, and high photoelectric conversion ability, $g\text{-C}_3\text{N}_4$ has attracted much interest in the construction of PEC biosensors. However, the relatively poor charge conductivity and the higher recombination rate of electrons and holes substantially influence the applications of $g\text{-C}_3\text{N}_4$ in PEC sensing.

Addressing the aforementioned issues, various approaches have been proposed to improve the photoelectric properties of $g\text{-C}_3\text{N}_4$ nanomaterial. For instance, ultrathin 2D nanosheets that were reduced from bulk C_3N_4 were used for the sensitive PEC detection of small molecular compounds [97]. Considering the fact that the recombination of photogenerated charge carriers generated from graphitic carbon nitride can be efficiently inhibited by the nitrogen vacancies, Li et al. prepared nitrogen-deficient graphitic carbon nitride-modified ITO electrodes, which were used for highly sensitive PEC analysis of ciprofloxacin [98]. Besides, heteroatom doping is another valid strategy to enhance the photoelectric activity [99]. To do so, Wang et al. prepared $\text{Cd/N@g-C}_3\text{N}_4$ photoactive nanomaterial by coupling the N_2 plasma treatment with the deposition of a Cd probe. The doping of N significantly enhanced the PEC response of the yielded nanocomposite to H_2S , due to the formation of an efficient Z-scheme heterojunction followed by the in-situ generation of CdS. On the basis of the high charge transport property between CdS and $g\text{-C}_3\text{N}_4$ resulting from the doped N, a “signal on” PEC sensing platform for H_2S was constructed [100]. Using a similar strategy, and employing a Z-scheme heterojunction of $\text{CoO/Au/g-C}_3\text{N}_4$ as the photoactive nanomaterial, Zeng et al. proposed a PEC aptasensor for the sensing of MC-LR based on the increment of photocurrent responses caused by the target-triggered consumption of photogenerated holes. In this work, the Z-scheme heterojunction was well fabricated because of the perfectly matched bandgaps of CoO and $g\text{-C}_3\text{N}_4$ coupled with the imbedded Au NPs, which not only served as the electron transfer media but also improved the visible light-harvesting ability of the nanohybrid because of the SPR effect [101]. Apart from the abovementioned binary heterostructures, multiple $g\text{-C}_3\text{N}_4$ -based heterostructures have also been reported to develop PEC biosensors [102]. For instance, through the in-situ growth approach, Wei et al. fabricated an SnO_2 - and SnS_2 -modified mesoporous $g\text{-C}_3\text{N}_4$ ($\text{SnO}_2/\text{SnS}_2/\text{mpg-C}_3\text{N}_4$) nanohybrid, which resulted in the significant improvement of PEC responses in contrast with their single materials or binary hybrids due to the well-matched bandgaps. By employing PbS/SiO_2 -labelled secondary antibody as the quencher, a PEC immunosensor with a sandwich structure was

constructed for the sensing of N-terminal pro-brain natriuretic peptide [103]. Similarly, using $\text{TiO}_2/\text{g-C}_3\text{N}_4/\text{CdS}$ composite to serve as a photoactive matrix and CdSe QDs as a sensitizer, Zhu et al. fabricated an ultrasensitive PEC detection platform for the sensing of T4 polynucleotide kinase based on the target-triggered sensitization of CdSe QDs, and the detection limit was shown to be $2.5 \text{ pg}\cdot\text{mL}^{-1}$ [104]. In addition to coupling with inorganic semiconductors, the photoelectric property of $\text{g-C}_3\text{N}_4$ can also be enhanced by organic modification. For instance, on the basis of π -stacking interactions, Song et al. fabricated a $\text{g-C}_3\text{N}_4$ -functionalized two-dimensional (2D) pyrene covalent organic framework (PAF-130/ $\text{g-C}_3\text{N}_4$), which exhibited substantially enhanced photoelectric conversion efficiency due to the efficient separation of photogenerated electrons and holes resulting from the well-matched bandgaps between PAF-130 and $\text{g-C}_3\text{N}_4$. This novel nanohybrid demonstrated promising potential in the construction of ultrasensitive PEC bioassay platforms [105].

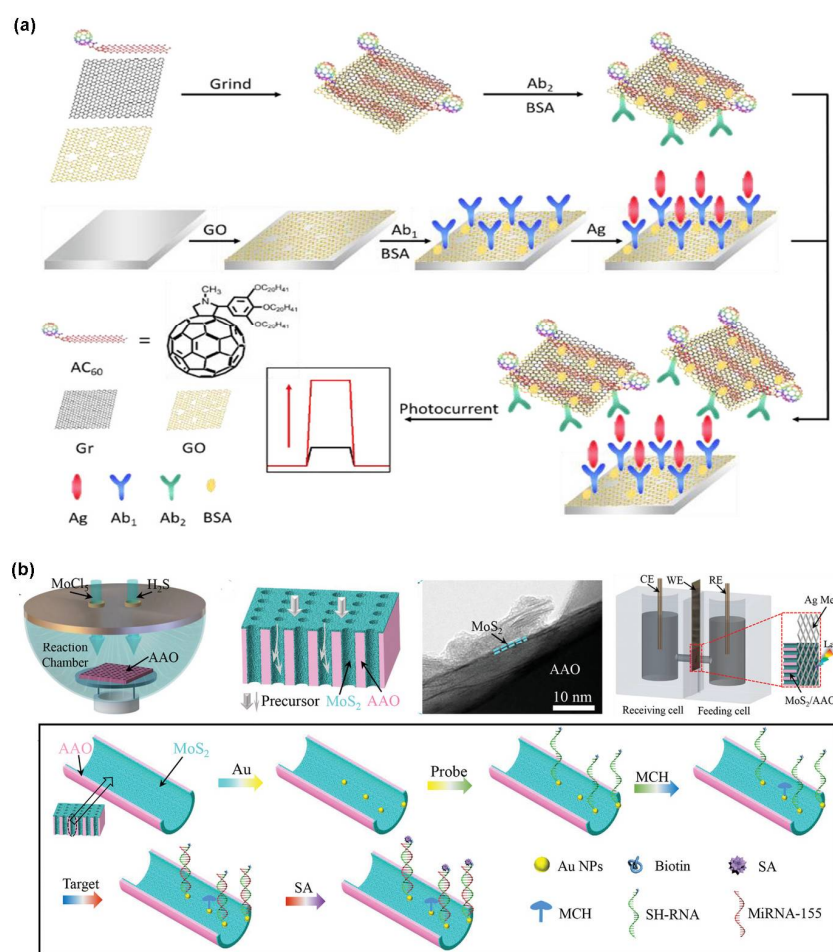


Figure 4. (a) Scheme of general processes for the assembly of AC_{60} -Gr-GO and construction of the PEC AFP immunosensor. Reprinted with permission from ref. [95]. Copyright 2018, American Chemical Society; (b) schematic illustration of the construction of a PEC biosensor based on the MoS_2/AAO photoactive nanochannel. Reprinted with permission from ref. [106]. Copyright 2020, John Wiley and Sons.

2.3.2. Transition Metal Dichalcogenides (TMDs)

As one of the most important families of 2D nanostructures, TMDs present a laminated structure with a chemical formula of MX_2 . Here, M represents the transition metal elements, particularly molybdenum (Mo) and tungsten (W), and X refers to chalcogen, such as sulfur (S), selenium (Se), and tellurium (Te). Similar to graphene, TMDs exhibit layered 2D nanostructures, which highly increases their surface area and efficiently closes the transfer distance of photogenerated charge carriers.

Among the various TMD nanomaterials, MoS₂ has received the most concerns in the applications of PEC bioassay due to its high optical absorption coefficient and long photoexcited carrier lifetimes. However, limited by the high recombination efficiency of photogenerated electron–hole pairs, hybridizing 2D nanostructures of MoS₂ with another compound is a great approach to acquire higher analytical performances. Taking Au NPs, for example, Liu et al. proposed an ultrasensitive PEC sensor for miRNA-155 assay using the photoactive anodic aluminum oxide (AAO) nanochannels functionalized with Au NP-deposited MoS₂ flakes. As shown in Figure 4b, MoS₂ film was modified on the channel of AAO by atomic layer deposition (ALD). The following decorating of Au NPs not only enhanced the photoelectric conversion efficiency of MoS₂ because the Au/MoS₂ Schottky junction might have efficiently improved the separation of electron–hole pairs, but also facilitated the immobilization of bio-recognition elements. Employing MoS₂/AAO-connected silver mesh as the working electrode, the detection limit of the proposed biosensor was shown to be 3 aM based on the steric effect [106]. Except for the noble-metal NPs sensitization, the constructing heterojunction is another way to improve the performances of MoS₂-based PEC biosensing applications. With this consideration, based on the well-matched bandgaps of n-type ZnO nanorods and p-type MoS₂ flakes, Niu et al. fabricated a MoS₂/ZnO heterostructure that greatly improved its light-harvesting ability and accelerated the separation of photogenerated charge carriers as well. The as-prepared heterostructure-modified ITO photoactive electrodes were successfully used for the highly selective detection of propyl gallate (PG) on account of the specific recognition of Zn (II) and oxygen atoms of PG [107]. As we know, dye sensitization is beneficial for nanomaterials to improve their light-response activities [108]. For example, the bandwidth of MoS₂ nanosheets would be obviously narrowed after being decorated with zinc phthalocyanine NPs (ZnPc NPs). Furthermore, in contrast with MoS₂, the fabricated ZnPc/MoS₂ nanohybrid received a two-fold improvement in carrier lifetime and a 24-fold increment in photocurrent intensity under visible light illumination [109]. In addition, 2D MoS₂ can also serve as the nanoprobe for the construction of PEC bioassay architectures [110].

A layered WS₂ nanostructure is another kind of TMD of extensive interest that has a narrow bandgap of about 1.3 eV and a large specific area [111]. However, its relatively high recombination efficiency of photogenerated charge carriers is still a tough challenge in PEC biosensing applications. Addressing this issue, combining WS₂ with appropriate functional nanomaterials is a widely reported approach to improve the PEC performance [112,113]. For example, considering the well-matched bandgaps of WS₂ and g-C₃N₄, Yin et al. fabricated an Au NP-decorated C₃N₄-WS₂ heterojunction that demonstrated a significantly improved photoelectric conversion property resulting from the notably improved transport rate of electrons and the efficient separation of photogenerated electrons and holes. The as-prepared photoactive nanohybrid was employed to construct a sensitive PEC DNA-sensing platform based on the target DNA, which induced the capture of MnO₂ nanoflowers that suppressed the photocurrents by the consumption of the electron donor [114]. For another example, Yin et al. employed the composition of MoS₂ nanosheet- and WS₂ nanosheet-modified ITO as the photoactive electrodes and the amino-functionalized Fe₂O₃ and SMCC as the linker. After 4-amino-3-hydrazino-5-mercapto-1,2,4-triazole (AHMT) was fixed on the photoelectrode, the target 5-formylcytosine (5fC) was captured by AHMT, which further triggered the immobilization of black TiO₂ (B-TiO₂) on the surface of the WS₂/MoS₂/ITO electrode. In this way, the target-controlled increase in photocurrent signal was monitored due to the generation of a B-TiO₂/WS₂MoS₂/ITO ternary heterojunction, which significantly enhanced the transport rate of the photogenerated charge carriers and extended their lifetimes, as well [115].

2.4. 3D-Nanostructure Materials

The 3D-nanostructure materials discussed here typically refer to the single architecture constructed by 0D-, 1D-, and 2D-nanoscale materials [6]. Currently, 3D architectures have attracted growing interest in PEC bioassays [116–118] because their carefully fabricated

hierarchical and biomimetic architectures usually exhibit many attractive advantages, such as excellent target-capture ability, outstanding signal-amplification properties, higher catalytic activity, and notable sensing performances. Structured according to the chemical compositions, different 3D architectures with morphologies like mimicking flowers, coral, and rich wrinkles, which have been widely reported in PEC biosensing, will be discussed in the following part.

Under elaborated preparation, various metal chalcogenides with 3D biological hierarchical architectures have been employed in PEC sensing applications due to their fantastic electrical and optical properties [119,120]. As demonstrated in Figure 5, a peony-like MoS_2 nanosheet directly growing on the nanohole-patterned TiO_2 was fabricated by Mahshid et al. After the further deposition of Au NPs, the light-absorption region of the hybrid was broadened to 700 nm, resulting from the outstanding electronic conductivity and SPR effect of the Au NPs. Based on the special morphology and the excellent PEC property of the prepared 3D MoS_2/Au hybrid, the detection limit for glucose was 1.3 nM [121].

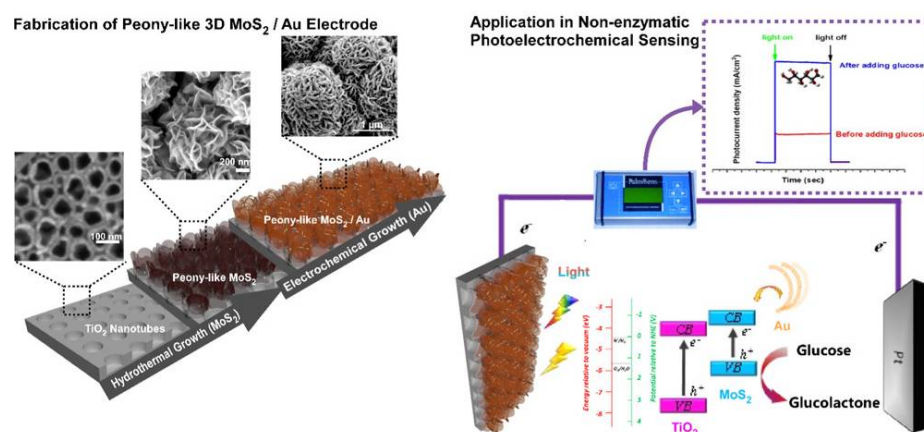


Figure 5. Nanopattern-assisted direct growth of binary MoS_2/gold electrode and the PEC process for glucose detection by peony-like 3D MoS_2/Au . Reprinted with permission from ref. [121]. Copyright 2020, American Chemical Society.

Other examples of 3D architectures that have been reported for use in PEC biosensing are ternary compound semiconductors. For example, ZnIn_2S_4 with 3D architectures have drawn much interest in PEC bioassay applications due to their low cost, high chemical stability, and great visible light-harvesting properties. However, the relatively short lifetime of photogenerated charge carriers is still a great challenge that 3D ZnIn_2S_4 architectures face. Addressing this issue, Li et al. proposed a lanthanum-doped CdS-immobilized flower-like ZnIn_2S_4 -modified $\text{Au}@\text{ZnO}$ photoactive electrode ($\text{La-CdS}/\text{ZnIn}_2\text{S}_4/\text{Au}@\text{ZnO}$) for the sensitive detection of aminoterminal pro-brain natriuretic peptides (NT-proBNP) based on the steric effect. The La-CdS with a narrow bandgap significantly improved the visible light-absorption efficiency and efficiently suppressed the recombination of photogenerated electron–hole pairs, which greatly enhanced the PEC biosensing performances of the 3D ZnIn_2S_4 -based photoactive materials [122]. Zhang et al. fabricated a Schottky junction by decorating Bi NPs on the hollow porous ZnSnO_3 microspheres (Bi/ZnSnO_3), which have much more electron-transport channels and abundant active sites for surface recognition. On account of the SPR effect of metallic Bi NPs, the number of photogenerated charge carriers of the Bi/ZnSnO_3 composite was significantly increased, which greatly improved the photocurrent intensity of the as-prepared photoactive material. Furthermore, compared with pure ZnSnO_3 , the light-absorption edge of Bi/ZnSnO_3 was broadened from 397 nm to the near-infrared region, as well. Based on the specific chelating coordination interaction between the target of norepinephrine (NE) and Zn^{2+} coupled with the high photoelectric activity of the Bi/ZnSnO_3 composite, an ultrasensitive and highly selective PEC biosensing platform was successfully constructed [123].

Apart from the abovementioned metal-based 3D architectures, various carbon-based 3D architectures also presented promising prospects. Taking 3D nitrogen-doped graphene hydrogel (3DNGH), for example, the analyte-trapping performance was dramatically improved because of its porous hierarchical structure, which offers abundant active sites. Besides, the doping of N is beneficial for enhancing its light-harvesting property and accelerating the separation of photogenerated electrons and holes [124]. Another interesting example is Gong et al., who proposed a coral-like g-C₃N₄ that had been applied to PEC detection of metronidazole (MNZ) in medicine samples. Through the morphology control, the coral-like g-C₃N₄ with an interlaced porous network structure demonstrated particular effects on antibody anchoring, electron transport, and the separation of electron-hole pairs [125]. In another study, flower-like Au-decorated 3D reduced graphene oxide (3D-rGO) was fabricated on the substrate of paper cellulose fiber for the construction of a chemiluminescence-driven PEC lab on a paper platform. In contrast with 2D architecture, the enlarged specific surface area of the 3D-rGO greatly facilitated the immobilization of functional groups. Furthermore, the corrugated 3D architecture was beneficial for efficient mass and electron transfer, which provided a guarantee to construct the ultrasensitive PEC thrombin biosensor [126].

Some examples of 0D-, 1D-, 2D-, and 3D-nanostructure materials for PEC sensing applications are summarized in Table 1 for intuitive comparison.

Table 1. Summary of representative nanostructure materials for PEC analysis discussed in this review.

Nanostructure	Feature	Material	Target	Ref.
0D				
QDs	Easily regulated bandgaps, excellent surface modification property and similar size to many biomolecules	CdTe QDs	CA125	[16]
		ZnS@Ag ₂ S QDs	Hg ²⁺	[17]
		DNA TET-CdTe QDs-MB	miRNA-141	[18]
		TPP doped Pdots	Telomerase activity	[23]
Carbon-based NPs	Low cytotoxicity, resistance to photobleaching, and fascinating biocompatibility	N-doped C-dots	CEA	[38]
		GOD@Con-A	N-glycan expression on the surface of MCF-7 cells	[44]
Noble-metal NPs	Easy to synthesize in different sizes, excellent stability and biocompatibility	ZnO NDs@g-C ₃ N ₄ QDs	CCRF-CEM cell	[46]
		Au NCs-Ag@SiO ₂	Alkaline phosphatase activity	[50]
		Au@Ag NPs-TiO ₂ NRs	DNA	[52]
		Ag@Au asymmetric core-satellite	PSA	[57]
1D				
Metal-oxide NWs	Strong light absorption property, low toxicity, and high chemical stability and biocompatibility	TiO ₂ NWs	Glucose	[70]
		TiO ₂ nanoneedles @MoO ₃	RAW264.7 cells	[71]
		ZnO NRs-CdTe QDs	DNA sequence of HIV-1	[72]
		Fe ₂ O ₃ NRs-Au NPs	lysozyme	[73]
Metal-chalcogenide NRs	Narrow bandgaps, significantly increased binding sites, and decreased radial transport distance	β-CD@CdS NRs	DNA sequence of HIV	[77]
		Pt SAs/CdS NRs	PSA	[80]
		Bi ₂ S ₃ NRs	PNK	[83]
Carbon NTs	Excellent photogenerated electron-transfer property	TiO ₂ NPs@CNTs	MC-LR	[85]
		MIL-68(In)-NH ₂ /MWCNT/CdS NPs	Tc	[86]
		Au NPs/CNTs	CEA	[87]
2D				
Carbon-based graphene-like nanostructures	Outstanding electron conductivity and high specific surface area	Bi ₂ MoO ₆ /BNG	Lincomycin	[91]
		PCN-224/rGO	p-ASA	[93]
		AC ₆₀ -Gr-GO	AFP	[95]
		CoO/Au NPs/g-C ₃ N ₄	MC-LR	[101]
		SnO ₂ /SnS ₂ /mpg-C ₃ N ₄	N-terminalpro-brain natriuretic peptide	[103]
		TiO ₂ /g-C ₃ N ₄ /CdS	T4 polynucleotide kinase	[104]
TMDs	High specific surface area and short photogenerated charge-carrier transfer distance	PAF-130/g-C ₃ N ₄	α-synuclein	[105]
		AAO-MoS ₂ film	miRNA-155	[106]
		MoS ₂ flakes-ZnO NRs	PG	[107]
		ZnFe NPs-MoS ₂ Nanosheets	Edifenphos	[109]
		Au NPs-C ₃ N ₄ -WS ₂ nanosheets	5fC	[114]
		WS ₂ -MoS ₂ nanosheets	5fC	[115]
3D				
Metal chalcogenides	Mimicking flower-like morphologies and excellent target-capture ability	Peony-like MoS ₂ Nanosheet Au NPs	Glucose	[121]
Ternary compound semiconductors	Low cost, high chemical stability, and great visible light-harvesting property	La-CdS-ZnIn ₂ S ₄ -Au@ZnO	NT-proBNP	[122]
		Bi NPs-ZnSnO ₃ microspheres	NE	[123]
Carbon-based architectures	Abundant active sites, high light-harvesting property, and fast charge-carrier transfer speed	Coral-like g-C ₃ N ₄	MNZ	[125]
		Flower-like Au-3D-rGO	Thrombin	[126]

3. Novel PEC Biosensing Patterns

In the past few decades, PEC biosensing has made great advances due to its distinct advantages of high sensitivity, easy operation, low cost, and increased flexibility. However, considering the increasing demands for portability and the integration of sensing devices, the development of novel PEC biosensing patterns with even greater performance has become more and more urgent. Therefore, a series of relevant reported research works will be discussed in this part.

3.1. Mimic Enzyme Assay

Due to the excellent specificity, natural enzymes have been widely used in PEC bioassays. However, the poor stability, tedious preparation, and relatively high prices are the main challenges to their further application. In recent years, it has been found that some nanomaterials such as metal NPs [127], carbon materials [128,129], and metal oxides [130] can demonstrate enzyme-like characteristics. Because of the excellent stability, high catalytic activity, and low cost, nanomaterial-based mimic enzymes have attracted great research interest in the construction of PEC analytical platforms.

Among various artificial enzymes, horseradish peroxidase (HRP)-like mimic enzymes are the most commonly used catalysts during PEC biosensing applications. For instance, Zhang et al. synthesized manganese-based mimic enzyme (MnME) that could catalyze the oxidation of DAB to produce insulating precipitate due to its excellent peroxidase-like activity. Using Au NP-decorated MnME as the nanoprobe and Au NP-modified Bi₂S₃ nanorods as the photoactive material, a highly sensitive “signal off” PEC biosensor for polynucleotide kinase activity was proposed (Figure 6a) [83]. Based on the similar mimic enzyme catalytic precipitation strategy, numerous advances in nanozyme research have been reported [112,131–134]. In addition, according to mimic enzyme-induced in situ generation of electron acceptors or donors, Dai et al. proposed a “signal on” PEC biosensor for the detection of H₂O₂ in vitro by using G-quadruplex/hemin/Pt NP nanocomposite as the catalyst. Specifically, after being anchored on the surface of C₃N₄ nanosheet/PbS QDs/ITO electrode, the as-prepared mimic enzyme catalyzed the oxidation of H₂O₂ to generate the electron donor of O₂, which accelerated the separation of photogenerated electrons and holes and eventually improved the photocurrent intensities [135].

Recently, except for the abovementioned peroxidase mimic enzymes, RNA-cleaving DNA enzymes (DNAzymes) have demonstrated promising results due to their advantages of great stability and excellent specificity [136]. With the activation of metal ions, DNAzymes catalyzed substrate strands to cleave into two fragments at the position of RNA [136,137]. For instance, on the basis of target Pb²⁺ triggering the cleave of substrate strand DNA1 resulting from the catalysis of CdS QD-modified DNAzyme (DNA2-Cd QD), which significantly suppressed the photocurrent signals due to the disassembly of the TiO₂/Au/CdS QD-constructed “Z-scheme”, Chen et al. developed a novel PEC sensor for the detection of Pb²⁺ with the detection limit calculated to be 0.13 pM [138].

3.2. Self-Powered Sensing

With the constantly emerging numerous splendid signal strategies, PEC analysis has attracted great interest in the biosensing field. However, to meet the request of clinical applications, the development of portable and simple instruments is urgently needed. Recently, self-powered sensors, which can work without external power supplies, have aroused increasing interest in biosensing applications. Different from traditional PEC sensing devices, self-powered PEC biosensors usually employ two electrodes that serve as the photoanode and photocathode. Under illumination, the current intensities, which result from the oxidation occurring on the photoanode coupled with the reduction occurring on the photocathode, respond to concentrations of the targets and highly sensitive self-powered assays can be achieved. For example, with the tyrosinase (Tyr)-triggered oxidation of phenol, the generation of catechol serving as the electron donor significantly improved the photocurrent response of the g-C₃N₄-Bi₂S₃ photoanode. Based on this, and combined

with the tris (2-carboxyethyl) phosphine (TCEP)-induced chemical redox cycling of catechol, an ultrasensitive and selective self-powered PEC biosensor for Tyr was developed [139]. The traditional PEC assay in particular can be converted into a self-powered PEC assay by the regulation of electron acceptors or donors. For instance, as the working electrode, Au NP @ZnSe nanosheet-modified gold electrodes (Au NPs @ZnSe NSs/GE) only had very low photocurrent signals, as the bias voltage was at 0 V. However, with the electron acceptor of methylene blue (MB) and p-nitrophenol (p-NP) introduced into the electrolyte solution, the photocurrent intensities of the electrodes were greatly enhanced. Based on this, Hun et al. proposed a novel self-powered PEC sensor for sensing KLK2 and PCA3 [140]. Except for the regulation of the electrolyte solution, well-designed photoactive electrodes have been proven to be another efficient approach to constructing self-powered PEC sensors. As exhibited in Figure 6b, Tang et al. proposed a self-powered PEC biosensor for the detection of oxytetracycline (OTC) with a two-electrode system that included the Z-scheme nanostructure photoanode of $\text{WO}_3/\text{g-C}_3\text{N}_4/\text{MnO}_2$ and the aptamer-based photocathode of Au NP-decorated rGO. Owing to the excellent light-harvesting ability and the high separation efficiency of the electrons and holes of the prepared hybrid, the great electrical conductivity of Au NPs, and the abundant active sites of rGO, the detection limit of the as-fabricated self-powered PEC sensor was shown to be 0.1 pM [141].

3.3. Dual-Readout Assay

In contrast with single-readout protocol, dual-readout assays that couple PEC analysis with other simple and convenient sensing modes have attracted increasingly intense interest due to their highly improved accuracy resulting from intercalibration and widened linear ranges. Taking photothermal sensing, for example, and considering the target-induced concentration changes of the photothermal materials aroused notable changes in temperature, Dai et al. proposed a simple dual-readout sialic-acid sensor by employing TPP-Pdots as the integrated signal probe of PEC and photothermal sensing. On the basis of sandwich-type immune recognition, the targets were able to trigger an increment in photocurrent intensities and temperature signals [142]. Combining PEC sensing with other electrochemical detection modes is also an efficient approach to constructing dual-readout biosensors. For example, it was found that the catalytic precipitation property of AuPtPd nanozymes could be regulated by urease-induced proton-consuming reactions. Inspired by this, and employing BiVO_4 -modified ITO as the photoelectrode and AuPtPb nanospheres as peroxidase-like nanozymes, a photocurrent and electrochemical impedance signal-based dual-readout biosensor for the detection of urease activity was proposed [143]. In regard to coupling PEC sensing with electrochemiluminescence (ECL) strategy, based on the glutathione-triggered Mn^{2+} -dependent DNAzyme amplification and DNA walker-controlled immobilization of CdS:Mn-streptavidin probs, Jie et al. fabricated a versatile dual-readout ECL and PEC biosensor for glutathione determination in human serum samples [144]. Visual detections have drawn increasing interest due to the simple devices and convenient operation. Coupling naked-eye readout with PEC sensing not only guarantees the accuracy of results but also improves the detection efficiency. For example, using CuInS_2 microflower-modified ITO as photoactive electrodes and antibody-labelled chlorin e6 (Ce6) as upconversion nanomaterials, which served as both PEC and visible signal probes, a PEC and near-infrared (NIR)-driven fluorescence visualization biosensor for the immunoassay of PSA was constructed by Ouyang et al. based on target-triggered sandwich immunobinding (Figure 6c) [145].

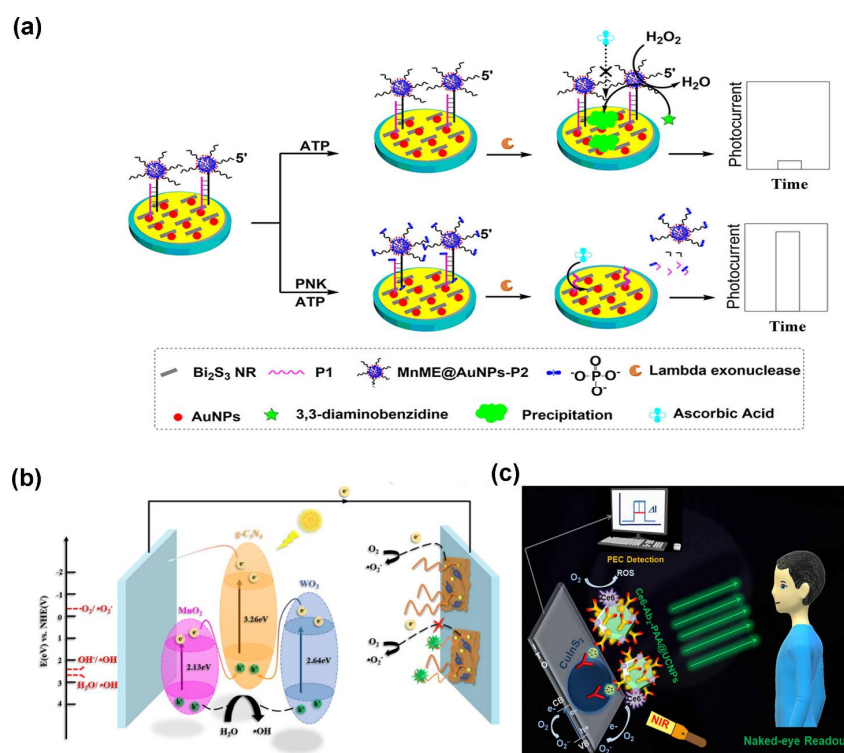


Figure 6. (a) Schematic illustration of a signal-on PEC biosensing for PNK assay based on the strategy of MnME@Au NP-P2 catalytic precipitation. Reprinted with permission from ref. [83]. Copyright 2018, American Chemical Society; (b) PEC mechanism of the self-powered photoanode-supported PEC cathodic sensing. Reprinted with permission from ref. [141]. Copyright 2021, American Chemical Society; (c) schematic illustration of the mechanism for the integrated NIR fluorescence-induced naked-eye readout and photoelectrochemical sensing. Reprinted with permission from ref. [145]. Copyright 2021, American Chemical Society.

4. Conclusions and Perspectives

With the substantial development of material technology and the high customization of biological systems, PEC biosensing has achieved great progress. According to remarkable advances in the last five years, this review summarized the functional nanostructured materials with different dimensionality employed in PEC bioanalysis. The morphology regulation of nanostructures plays a crucial role in the improvement of sensing performance. Compared with 0D, 1D, and 2D nanostructures, 3D-aligned arrays have more favorable electron transfer routes due to the multi-dimensional space and can offer larger surface area as well as uniform pore size for target capture and detection. Several novel PEC biosensing patterns with outstanding advantages in low cost, miniaturization, and high accuracy were also discussed. We sincerely hope this overview can serve as a useful source for interested readers.

As a newly developed sensing technology, PEC bioanalysis still has some challenges to overcome for the practical applications. For example, the fabrication of photoactive electrodes with more stable and higher performance will still be the focus of future works. Easy-operating and highly reproductive sensing patterns remain to be constructed to meet the demand of clinical diagnosis and industrial monitoring. Besides, in a way, the introduction of physical light sources into the PEC analysis system is still a challenge for the commercialization of PEC biosensors. According to the practical application demand and the recent research status, further research in PEC sensing has some trends, as follows. (1) Constructing a photoelectric functional interface by using novel photoactive materials or advanced preparation techniques—for instance, tailoring photoactive nanostructures with specific morphologies to improve the target-capture ability and exploit materials

with long-wavelength response to minimize the damage to biomolecules during the optical excitation. In addition, using novel fabrication techniques, such as screen printing and microelectromechanical systems for the preparation of electrodes, could efficiently suppress the interelectrode interferences and make it easy to carry out mass production. (2) Miniaturizing and highly integrating the PEC sensing instruments. In order to meet the requirements of low cost and fast and simple operation, great efforts are needed to streamline PEC sensing devices and further improve their portability. In this regard, many interesting attempts have been made, such as displacing a physical light source with chemiluminescence (CL) for the excitation of photoactive materials [146], employing a self-powered detection model without external power supplies [147], and developing a portable PEC sensing device by integrating a CL-based signal-generating system and a paper-based supercapacitor coupled with a digital multimeter reading system [148]. Even so, most of these studies are still in their preliminary exploratory stage. (3) Combining a PEC biosensor with multidisciplinary techniques to construct an integrated bioanalysis system. To meet the increasing demand for practical applications, integrating PEC analysis with other electronics or micromachining technologies is an effective approach. For instance, based on the inherent signal-amplification ability of organic electrochemical transistors (OECTs), Zhao et al. integrated one with a PEC biosensor and successfully realized the ultrasensitive detection of C-reactive protein. In contrast with traditional PEC biosensors, targets induced a change in the current signal of the novel OECT-PEC biosensor that was enhanced by nearly two orders of magnitude [149]. Nevertheless, as a developing field, there are many areas that need to be studied and improved, especially the signal mechanism under the irradiation of light. (4) Developing PEC nanotools for single-cell research. Considering the cell-to-cell differences, single-cell analysis is quite essential to reveal the behaviors and functions of each individual cell. Recently, a nanopipette whose tip was modified with an organic probe/NiO/Ni film was developed for intracellular drug delivery and further PEC assay of oxidative stress [150]. Although materials with high charges might not be loaded into cells by electroosmosis, this work still shows the bright prospects of PEC in single-cell analysis. In all, with the continuous advancement of science and substantial attempts, the present issues PEC assay is facing have the potential to be solved in the coming years.

Author Contributions: Conceptualization, L.Z., Y.-C.Z. and W.-W.Z.; investigation, L.Z. and Y.-C.Z.; writing—original draft preparation, L.Z. and Y.-C.Z.; writing—review and editing, L.Z. and Y.-C.Z.; visualization, L.Z., Y.-C.Z. and W.-W.Z.; supervision, W.-W.Z. All authors have read and agreed to the published version of the manuscript.

Funding: This work was funded by the National Natural Science Foundation of China (Grant Nos. 22004052 and 22104053) and the Scientific Research Foundation for high-level talents of the Jinling Institute of Technology (Grant No. jit-b-202160).

Institutional Review Board Statement: Not applicable.

Informed Consent Statement: Not applicable.

Data Availability Statement: Data sharing is not applicable to this article.

Conflicts of Interest: The authors declare no conflict of interest.

References

1. Becquerel, A.E. Recherches sur les effets de la radiation chimique de la lumiere solaire au moyen des courants electriques. *CR Acad. Sci.* **1839**, *9*, 1.
2. Ke, J.; He, F.; Wu, H.; Lyu, S.; Liu, J.; Yang, B.; Li, Z.; Zhang, Q.; Chen, J.; Lei, L.; et al. Nanocarbon-Enhanced 2D Photoelectrodes: A New Paradigm in Photoelectrochemical Water Splitting. *Nano-Micro Lett.* **2021**, *13*, 24. [[CrossRef](#)]
3. Mittal, H.; Khanuja, M. Hydrothermal in-situ synthesis of MoSe₂-polypyrrole nanocomposite for efficient photocatalytic degradation of dyes under dark and visible light irradiation. *Sep. Purif. Technol.* **2021**, *254*, 117508. [[CrossRef](#)]
4. Yu, S.-Y.; Zhang, L.; Zhu, L.-B.; Gao, Y.; Fan, G.-C.; Han, D.-M.; Chen, G.; Zhao, W.-W. Bismuth-containing semiconductors for photoelectrochemical sensing and biosensing. *Coord. Chem. Rev.* **2019**, *393*, 9–20. [[CrossRef](#)]

5. Svitková, V.; Palchetti, I. Functional polymers in photoelectrochemical biosensing. *Bioelectrochemistry* **2020**, *136*, 107590. [[CrossRef](#)]
6. Welch, E.C.; Powell, J.M.; Clevinger, T.B.; Fairman, A.E.; Shukla, A. Advances in Biosensors and Diagnostic Technologies Using Nanostructures and Nanomaterials. *Adv. Funct. Mater.* **2021**, *31*, 2104126. [[CrossRef](#)]
7. Tu, W.; Wang, Z.; Dai, Z. Selective photoelectrochemical architectures for biosensing: Design, mechanism and responsibility. *Trac Trends Anal. Chem.* **2018**, *105*, 470–483. [[CrossRef](#)]
8. Pokropivny, V.; Skorokhod, V. Classification of nanostructures by dimensionality and concept of surface forms engineering in nanomaterial science. *Mater. Sci. Eng. C* **2007**, *27*, 990–993. [[CrossRef](#)]
9. Brus, L.E. A simple model for the ionization potential, electron affinity, and aqueous redox potentials of small semiconductor crystallites. *J. Chem. Phys.* **1983**, *79*, 5566–5571. [[CrossRef](#)]
10. Rossetti, R.; Nakahara, S.; Brus, L.E. Quantum size effects in the redox potentials, resonance Raman spectra, and electronic spectra of CdS crystallites in aqueous solution. *J. Chem. Phys.* **1983**, *79*, 1086–1088. [[CrossRef](#)]
11. Willner, I.; Patolsky, F.; Wasserman, J. Photoelectrochemistry with controlled DNA-cross-linked CdS nanoparticle arrays. *Angew. Chem.* **2001**, *40*, 1861–1864. [[CrossRef](#)]
12. Esteve-Turrillas, F.; Abad-Fuentes, A. Applications of quantum dots as probes in immunosensing of small-sized analytes. *Biosens. Bioelectron.* **2013**, *41*, 12–29. [[CrossRef](#)]
13. Zhao, W.-W.; Yu, X.-D.; Xu, J.-J.; Chen, H.-Y. Recent advances in the use of quantum dots for photoelectrochemical bioanalysis. *Nanoscale* **2016**, *8*, 17407–17414. [[CrossRef](#)]
14. Zhou, H.; Liu, J.; Zhang, S. Quantum dot-based photoelectric conversion for biosensing applications. *Trac Trends Anal. Chem.* **2015**, *67*, 56–73. [[CrossRef](#)]
15. Dos Santos, M.C.; Hildebrandt, N. Recent developments in lanthanide-to-quantum dot FRET using time-gated fluorescence detection and photon upconversion. *TrAC Trends Anal. Chem.* **2016**, *84*, 60–71. [[CrossRef](#)]
16. Xue, H.; Zhao, J.; Zhou, Q.; Pan, D.; Zhang, Y.; Zhang, Y.; Shen, Y. Boosting the Sensitivity of a Photoelectrochemical Immunoassay by Using SiO₂@polydopamine Core–Shell Nanoparticles as a Highly Efficient Quencher. *ACS Appl. Nano Mater.* **2019**, *2*, 1579–1588. [[CrossRef](#)]
17. Zhang, L.; Lib, P.; Fengbc, L.; Chenbc, X.; Jiangb, J.; Zhangb, S.; Zhangb, C.; Zhangd, A.; Chena, G.; Wang, H. Synergetic Ag₂S and ZnS quantum dots as the sensitizer and recognition probe: A visible light-driven photoelectrochemical sensor for the “signal-on” analysis of mercury (II). *J. Hazard. Mater.* **2020**, *387*, 121715. [[CrossRef](#)]
18. Li, M.; Xiong, C.; Zheng, Y.; Liang, W.; Yuan, R.; Chai, Y. Ultrasensitive Photoelectrochemical Biosensor Based on DNA Tetrahedron as Nanocarrier for Efficient Immobilization of CdTe QDs–Methylene Blue as Signal Probe with Near-Zero Background Noise. *Anal. Chem.* **2018**, *90*, 8211–8216. [[CrossRef](#)]
19. Li, Y.; Zhang, N.; Zhao, W.-W.; Jiang, D.-C.; Xu, J.-J.; Chen, H.-Y. Polymer Dots for Photoelectrochemical Bioanalysis. *Anal. Chem.* **2017**, *89*, 4945–4950. [[CrossRef](#)]
20. Shi, X.-M.; Mei, L.-P.; Wang, Q.; Zhao, W.-W.; Xu, J.-J.; Chen, H.-Y. Energy Transfer between Semiconducting Polymer Dots and Gold Nanoparticles in a Photoelectrochemical System: A Case Application for Cathodic Bioanalysis. *Anal. Chem.* **2018**, *90*, 4277–4281. [[CrossRef](#)]
21. Zhang, N.; Shi, X.-M.; Guo, H.-Q.; Zhao, X.-Z.; Zhao, W.-W.; Xu, J.-J.; Chen, H.-Y. Gold Nanoparticle Couples with Entropy-Driven Toehold-Mediated DNA Strand Displacement Reaction on Magnetic Beads: Toward Ultrasensitive Energy-Transfer-Based Photoelectrochemical Detection of miRNA-141 in Real Blood Sample. *Anal. Chem.* **2018**, *90*, 11892–11898. [[CrossRef](#)]
22. Shi, X.-M.; Mei, L.-P.; Zhang, N.; Zhao, W.-W.; Xu, J.-J.; Chen, H.-Y. A Polymer Dots-Based Photoelectrochemical pH Sensor: Simplicity, High Sensitivity, and Broad-Range pH Measurement. *Anal. Chem.* **2018**, *90*, 8300–8303. [[CrossRef](#)]
23. Zhang, L.; Shi, X.-M.; Xu, Y.-T.; Fan, G.-C.; Liang, Y.-Y.; Wang, C.; Zhao, W.-W. Gold Nanoparticle-Induced Photocurrent Quenching and Recovery of Polymer Dots: Toward Signal-On Energy-Transfer-Based Photocathodic Bioanalysis of Telomerase Activity in Cell Extracts. *Anal. Chem.* **2019**, *91*, 6403–6407. [[CrossRef](#)]
24. Wang, Q.; Ruan, Y.-F.; Zhao, W.-W.; Lin, P.; Xu, J.-J.; Chen, H.-Y. Semiconducting Organic–Inorganic Nanodots Heterojunctions: Platforms for General Photoelectrochemical Bioanalysis Application. *Anal. Chem.* **2018**, *90*, 3759–3765. [[CrossRef](#)]
25. Liu, S.; Zhao, S.; Tu, W.; Wang, X.; Wang, X.; Bao, J.; Wang, Y.; Han, M.; Dai, Z. A “Signal On” Photoelectrochemical Biosensor Based on Bismuth@N,O-Codoped-Carbon Core-Shell Nanohybrids for Ultrasensitive Detection of Telomerase in HeLa Cells. *Chem. Eur. J.* **2018**, *24*, 3677–3682. [[CrossRef](#)]
26. You, F.H.; Wei, J.; Cheng, Y.; Wen, Z.R.; Ding, C.F.; Guo, Y.S.; Wang, K. A sensitive and stable visible-light-driven photoelectrochemical aptasensor for determination of oxytetracycline in tomato samples. *J. Hazard. Mater.* **2020**, *398*, 122944. [[CrossRef](#)]
27. Dong, Y.-X.; Cao, J.-T.; Wang, B.; Ma, S.-H.; Liu, Y.-M. Spatial-Resolved Photoelectrochemical Biosensing Array Based on a CdS@g-C₃N₄ Heterojunction: A Universal Immunosensing Platform for Accurate Detection. *ACS Appl. Mater. Interfaces* **2018**, *10*, 3723–3731. [[CrossRef](#)]
28. Hao, N.; Hua, R.; Zhang, K.; Lu, J.; Wang, K. A Sunlight Powered Portable Photoelectrochemical Biosensor Based on a Potentiometric Resolve Ratiometric Principle. *Anal. Chem.* **2018**, *90*, 13207–13211. [[CrossRef](#)]
29. Wang, Y.; Cheng, Y.; Wu, N.; Zhang, Z. Graphitic Carbon Nitride/Poly(3-Hexylthiophene) Nanocomposites for the Photoelectrochemical Detection of H₂O₂ in Living Cells. *ACS Appl. Nano Mater.* **2020**, *3*, 8598–8603. [[CrossRef](#)]

30. Zheng, Y.-N.; Liang, W.-B.; Xiong, C.-Y.; Yuan, Y.-L.; Chai, Y.-Q.; Yuan, R. Self-Enhanced Ultrasensitive Photoelectrochemical Biosensor Based on Nanocapsule Packaging Both Donor–Acceptor-Type Photoactive Material and Its Sensitizer. *Anal. Chem.* **2016**, *88*, 8698–8705. [[CrossRef](#)]
31. Shen, C.; Lou, Q.; Zang, J.; Liu, K.; Qu, S.; Dong, L.; Shan, C. Near-Infrared Chemiluminescent Carbon Nanodots and Their Application in Reactive Oxygen Species Bioimaging. *Adv. Sci.* **2020**, *7*, 1903525. [[CrossRef](#)]
32. Liu, H.; Sun, Y.; Li, Z.; Yang, J.; Aryee, A.A.; Qu, L.; Du, D.; Lin, Y. Lysosome-targeted carbon dots for ratiometric imaging of formaldehyde in living cells. *Nanoscale* **2019**, *11*, 8458–8463. [[CrossRef](#)] [[PubMed](#)]
33. Lan, M.; Zhao, S.; Zhang, Z.; Yan, L.; Guo, L.; Niu, G.; Zhang, J.; Zhao, J.; Zhang, H.; Wang, P.; et al. Two-photon-excited near-infrared emissive carbon dots as multifunctional agents for fluorescence imaging and photothermal therapy. *Nano Res.* **2017**, *10*, 3113–3123. [[CrossRef](#)]
34. Campuzano, S.; Yanez-Sedeno, P.; Pingarron, J.M. Carbon Dots and Graphene Quantum Dots in Electrochemical Biosensing. *Nanomaterials* **2019**, *9*, 634. [[CrossRef](#)] [[PubMed](#)]
35. Song, Y.; Ostermeyer, G.P.; Du, D.; Lin, Y. Carbon nanodot-hybridized silica nanospheres assisted immunoassay for sensitive detection of Escherichia coli. *Sens. Actuators B Chem.* **2021**, *349*, 130730. [[CrossRef](#)]
36. Putri, F.A.R.; Mudasar, M.; Morita, K.; Suherman, S. Microwave-Assisted Synthesis of Amikacin Modified N,S co-Doped Carbon Dots for Escherichia coli Detection. *Chemosensors* **2019**, *7*, 61. [[CrossRef](#)]
37. da Silva, J.C.E.; Gonçalves, H.M. Analytical and bioanalytical applications of carbon dots. *TrAC Trends Anal. Chem.* **2011**, *30*, 1327–1336. [[CrossRef](#)]
38. Li, L.; Wang, T.; Zhang, Y.; Xu, C.; Zhang, L.; Cheng, X.; Liu, H.; Chen, X.; Yu, J. Editable TiO₂ Nanomaterial-Modified Paper in Situ for Highly Efficient Detection of Carcinoembryonic Antigen by Photoelectrochemical Method. *ACS Appl. Mater. Interfaces* **2018**, *10*, 14594–14601. [[CrossRef](#)]
39. Sui, C.; Wang, T.; Zhou, Y.; Yin, H.; Meng, X.; Zhang, S.; Waterhouse, G.I.; Xu, Q.; Zhuge, Y.; Ai, S. Photoelectrochemical biosensor for hydroxymethylated DNA detection and T4- β -glucosyltransferase activity assay based on WS₂ nanosheets and carbon dots. *Biosens. Bioelectron.* **2019**, *127*, 38–44. [[CrossRef](#)]
40. Tang, L.; Ji, R.; Li, X.; Bai, G.; Liu, C.P.; Hao, J.; Lin, J.; Jiang, H.; Teng, K.S.; Yang, Z.; et al. Deep Ultraviolet to Near-Infrared Emission and Photoresponse in Layered N-Doped Graphene Quantum Dots. *ACS Nano* **2014**, *8*, 6312–6320. [[CrossRef](#)]
41. Yeh, T.-F.; Teng, C.-Y.; Chen, S.-J.; Teng, H. Nitrogen-Doped Graphene Oxide Quantum Dots as Photocatalysts for Overall Water-Splitting under Visible Light Illumination. *Adv. Mater.* **2014**, *26*, 3297–3303. [[CrossRef](#)]
42. Yin, Y.; Liu, Q.; Jiang, D.; Du, X.; Qian, J.; Mao, H.; Wang, K. Atmospheric pressure synthesis of nitrogen doped graphene quantum dots for fabrication of BiOBr nanohybrids with enhanced visible-light photoactivity and photostability. *Carbon* **2016**, *96*, 1157–1165. [[CrossRef](#)]
43. Jiang, D.; Du, X.; Zhou, L.; Li, H.; Wang, K. New Insights toward Efficient Charge-Separation Mechanism for High-Performance Photoelectrochemical Aptasensing: Enhanced Charge-Carrier Lifetime via Coupling Ultrathin MoS₂ Nanoplates with Nitrogen-Doped Graphene Quantum Dots. *Anal. Chem.* **2017**, *89*, 4525–4531. [[CrossRef](#)]
44. Ge, S.; Lan, F.; Liang, L.; Ren, N.; Li, L.; Liu, H.; Yan, M.; Yu, J. Ultrasensitive Photoelectrochemical Biosensing of Cell Surface N-Glycan Expression Based on the Enhancement of Nanogold-Assembled Mesoporous Silica Amplified by Graphene Quantum Dots and Hybridization Chain Reaction. *ACS Appl. Mater. Interfaces* **2017**, *9*, 6670–6678. [[CrossRef](#)]
45. Wang, W.; Yu, J.C.; Shen, Z.; Chan, D.K.L.; Gu, T. g-C₃N₄ quantum dots: Direct synthesis, upconversion properties and photocatalytic application. *Chem. Commun.* **2014**, *50*, 10148–10150. [[CrossRef](#)] [[PubMed](#)]
46. Pang, X.; Cui, C.; Su, M.; Wang, Y.; Wei, Q.; Tan, W. Construction of self-powered cytosensing device based on ZnO nanodisks@g-C₃N₄ quantum dots and application in the detection of CCRF-CEM cells. *Nano Energy* **2018**, *46*, 101–109. [[CrossRef](#)] [[PubMed](#)]
47. Shu, J.; Tang, D. Recent Advances in Photoelectrochemical Sensing: From Engineered Photoactive Materials to Sensing Devices and Detection Modes. *Anal. Chem.* **2020**, *92*, 363–377. [[CrossRef](#)] [[PubMed](#)]
48. Victorious, A.; Saha, S.; Pandey, R.; Soleymani, L. Enhancing the Sensitivity of Photoelectrochemical DNA Biosensing Using Plasmonic DNA Barcodes and Differential Signal Readout. *Angew. Chem. Int. Ed.* **2021**, *60*, 7316–7322. [[CrossRef](#)]
49. Cui, L.; Shen, J.; Li, C.-C.; Cui, P.-P.; Luo, X.; Wang, X.; Zhang, C.-Y. Construction of a Dye-Sensitized and Gold Plasmon-Enhanced Cathodic Photoelectrochemical Biosensor for Methyltransferase Activity Assay. *Anal. Chem.* **2021**, *93*, 10310–10316. [[CrossRef](#)]
50. Zhao, C.-Q.; Zhou, J.; Wu, K.-W.; Ding, S.-N.; Xu, J.-J.; Chen, H.-Y. Plasmonic Enhanced Gold Nanoclusters-Based Photoelectrochemical Biosensor for Sensitive Alkaline Phosphatase Activity Analysis. *Anal. Chem.* **2020**, *92*, 6886–6892. [[CrossRef](#)]
51. Ruan, Y.-F.; Zhang, N.; Zhu, Y.-C.; Zhao, W.-W.; Xu, J.-J.; Chen, H.-Y. Photoelectrochemical Bioanalysis Platform of Gold Nanoparticles Equipped Perovskite Bi₄NbO₈Cl. *Anal. Chem.* **2017**, *89*, 7869–7875. [[CrossRef](#)]
52. Zhang, L.; Shi, X.-M.; Xu, Y.-T.; Fan, G.-C.; Yu, X.-D.; Liang, Y.-Y.; Zhao, W.-W. Binding-induced formation of DNAzyme on an Au@Ag nanoparticles/TiO₂ nanorods electrode: Stimulating biocatalytic precipitation amplification for plasmonic photoelectrochemical bioanalysis. *Biosens. Bioelectron.* **2019**, *134*, 103–108. [[CrossRef](#)]
53. Zhu, Y.-C.; Zhang, N.; Ruan, Y.-F.; Zhao, W.-W.; Xu, J.-J.; Chen, H.-Y. Alkaline Phosphatase Tagged Antibodies on Gold Nanoparticles/TiO₂ Nanotubes Electrode: A Plasmonic Strategy for Label-Free and Amplified Photoelectrochemical Immunoassay. *Anal. Chem.* **2016**, *88*, 5626–5630. [[CrossRef](#)]
54. Zhao, W.-W.; Yu, P.-P.; Shan, Y.; Wang, J.; Xu, J.-J.; Chen, H.-Y. Exciton-Plasmon Interactions between CdS Quantum Dots and Ag Nanoparticles in Photoelectrochemical System and Its Biosensing Application. *Anal. Chem.* **2012**, *84*, 5892–5897. [[CrossRef](#)]

55. Tang, Y.; Liu, X.; Zheng, H.; Yang, L.; Li, L.; Zhang, S.; Zhou, Y.; Alwarappan, S. A photoelectrochemical aptasensor for aflatoxin B1 detection based on an energy transfer strategy between Ce-TiO₂@MoSe₂ and Au nanoparticles. *Nanoscale* **2019**, *11*, 9115–9124. [[CrossRef](#)]
56. Zhang, L.; Sun, Y.; Liang, Y.-Y.; He, J.-P.; Zhao, W.-W.; Xu, J.-J.; Chen, H.-Y. Ag nanoclusters could efficiently quench the photoresponse of CdS quantum dots for novel energy transfer-based photoelectrochemical bioanalysis. *Biosens. Bioelectron.* **2016**, *85*, 930–934. [[CrossRef](#)]
57. Zhu, Y.-C.; Xu, F.; Zhang, N.; Zhao, W.-W.; Xu, J.-J.; Chen, H.-Y. DNA sequence functionalized with heterogeneous core satellite nanoassembly for novel energy-transfer-based photoelectrochemical bioanalysis. *Biosens. Bioelectron.* **2017**, *91*, 293–298. [[CrossRef](#)]
58. Hung, C.M.; Le, D.T.T.; Van Hieu, N. On-chip growth of semiconductor metal oxide nanowires for gas sensors: A review. *J. Sci. Adv. Mater. Devices* **2017**, *2*, 263–285. [[CrossRef](#)]
59. Kolmakov, A.; Moskovits, M. Chemical sensing and catalysis by one-dimensional metal-oxide nanostructures. *Annu. Rev. Mater. Sci.* **2004**, *34*, 151–180. [[CrossRef](#)]
60. Fang, S.; Wang, D.; Wang, X.; Liu, X.; Kang, Y.; Yu, H.; Zhang, H.; Hu, W.; He, J.; Sun, H.; et al. Tuning the Charge Transfer Dynamics of the Nanostructured GaN Photoelectrodes for Efficient Photoelectrochemical Detection in the Ultraviolet Band. *Adv. Funct. Mater.* **2021**, *31*, 2103007. [[CrossRef](#)]
61. Guo, X.; Liu, S.; Yang, M.; Du, H.; Qu, F. Dual signal amplification photoelectrochemical biosensor for highly sensitive human epidermal growth factor receptor-2 detection. *Biosens. Bioelectron.* **2019**, *139*, 111312. [[CrossRef](#)]
62. Wang, D.; Chen, L.; Liu, J.; Guan, F.; Sun, R.; Jiang, L.; Feng, X. A Reliable Photoelectrochemical Bioassay System Based on Cathodic Reaction at a Solid-Liquid-Air Joint Interface. *Adv. Funct. Mater.* **2018**, *28*, 28. [[CrossRef](#)]
63. Fan, B.; Fan, Q.; Hu, L.; Cui, M.; Wang, X.; Ma, H.; Wei, Q. Polydopamine-PEG-Folic Acid Conjugate Film Engineered TiO₂ Nanotube Arrays for Photoelectrochemical Sensing of Folate Binding Protein. *ACS Appl. Mater. Interfaces* **2020**, *12*, 1877–1884. [[CrossRef](#)] [[PubMed](#)]
64. Chen, X.; Li, D.; Pan, G.; Zhou, D.; Xu, W.; Zhu, J.; Wang, H.; Chen, C.; Song, H. All-inorganic perovskite quantum dot/TiO₂ inverse opal electrode platform: Stable and efficient photoelectrochemical sensing of dopamine under visible irradiation. *Nanoscale* **2018**, *10*, 10505–10513. [[CrossRef](#)]
65. Deng, H.; Chai, Y.; Yuan, R.; Yuan, Y. In Situ Formation of Multifunctional DNA Nanospheres for a Sensitive and Accurate Dual-Mode Biosensor for Photoelectrochemical and Electrochemical Assay. *Anal. Chem.* **2020**, *92*, 8364–8370. [[CrossRef](#)]
66. Fu, B.; Zhang, Z. Periodical 2D Photonic-Plasmonic Au/TiO_x Nanocavity Resonators for Photoelectrochemical Applications. *Small* **2018**, *14*, e1703610. [[CrossRef](#)] [[PubMed](#)]
67. Gao, N.; Fan, B.; Li, L.; Sun, X.; Wang, X.; Ma, H.; Wei, Q.; Ju, H. Label-Free Antifouling Photoelectrochemical Sensing Strategy for Detecting Breast Tumor Cells Based on Ligand-Receptor Interactions. *ACS Appl. Bio Mater.* **2021**, *4*, 4479–4485. [[CrossRef](#)]
68. Sheng, X.; He, D.; Yang, J.; Zhu, K.; Feng, X. Oriented Assembled TiO₂ Hierarchical Nanowire Arrays with Fast Electron Transport Properties. *Nano Lett.* **2014**, *14*, 1848–1852. [[CrossRef](#)]
69. Feng, X.; Zhu, K.; Frank, A.J.; Grimes, C.A.; Mallouk, T.E. Rapid Charge Transport in Dye-Sensitized Solar Cells Made from Vertically Aligned Single-Crystal Rutile TiO₂ Nanowires. *Angew. Chem. Int. Ed.* **2012**, *51*, 2727–2730. [[CrossRef](#)]
70. Chen, L.; Sheng, X.; Wang, D.; Liu, J.; Sun, R.; Jiang, L.; Feng, X. High-Performance Triphase Bio-Photoelectrochemical Assay System Based on Superhydrophobic Substrate-Supported TiO₂ Nanowire Arrays. *Adv. Funct. Mater.* **2018**, *28*, 1801483. [[CrossRef](#)]
71. Pang, X.H.; Bian, H.J.; Su, M.H.; Ren, Y.Y.; Qi, J.N.; Ma, H.M.; Wu, D.; Hu, L.H.; Du, B.; Wei, Q. Photoelectrochemical Cytosensing of RAW264.7 Macrophage Cells Based on a TiO₂ Nanoneedles@MoO₃ Array. *Anal. Chem.* **2017**, *89*, 7950–7957. [[CrossRef](#)] [[PubMed](#)]
72. Wang, S.; Zhao, J.; Zhang, Y.; Yan, M.; Zhang, L.; Ge, S.; Yu, J. Photoelectrochemical biosensor of HIV-1 based on cascaded photoactive materials and triple-helix molecular switch. *Biosens. Bioelectron.* **2019**, *139*, 111325. [[CrossRef](#)]
73. Li, Z.; Su, C.; Wu, D.; Zhang, Z. Gold Nanoparticles Decorated Hematite Photoelectrode for Sensitive and Selective Photoelectrochemical Aptasensing of Lysozyme. *Anal. Chem.* **2018**, *90*, 961–967. [[CrossRef](#)]
74. Chen, Y.; Deng, W.; Tan, Y.; Xie, Q. CdS Quantum-Dots-Decorated V₂O₅ Nanosheets as Chemically Etchable Active Materials for Sensitive Photoelectrochemical Immunoassay of Carcinoembryonic Antigen. *ACS Appl. Mater. Interfaces* **2020**, *12*, 29066–29073. [[CrossRef](#)] [[PubMed](#)]
75. Zhu, Y.-C.; Xu, Y.-T.; Xue, Y.; Fan, G.-C.; Zhang, P.-K.; Zhao, W.-W.; Xu, J.-J.; Chen, H.-Y. Three-Dimensional CdS@Carbon Fiber Networks: Innovative Synthesis and Application as a General Platform for Photoelectrochemical Bioanalysis. *Anal. Chem.* **2019**, *91*, 6419–6423. [[CrossRef](#)]
76. Vaquero, F.; Navarro, R.; Fierro, J. Influence of the solvent on the structure, morphology and performance for H₂ evolution of CdS photocatalysts prepared by solvothermal method. *Appl. Catal. B Environ.* **2017**, *203*, 753–767. [[CrossRef](#)]
77. Fan, J.; Zang, Y.; Jiang, J.; Lei, J.; Xue, H. Beta-cyclodextrin-functionalized CdS nanorods as building modules for ultrasensitive photoelectrochemical bioassay of HIV DNA. *Biosens. Bioelectron.* **2019**, *142*, 111557. [[CrossRef](#)]
78. Li, Q.; Chen, W.; Xiao, H.; Gong, Y.; Li, Z.; Zheng, L.; Zheng, X.; Yan, W.; Cheong, W.; Shen, R.; et al. Fe Isolated Single Atoms on S, N Codoped Carbon by Copolymer Pyrolysis Strategy for Highly Efficient Oxygen Reduction Reaction. *Adv. Mater.* **2018**, *30*, e1800588. [[CrossRef](#)] [[PubMed](#)]
79. Wu, J.; Xiong, L.; Zhao, B.; Liu, M.; Huang, L. Densely Populated Single Atom Catalysts. *Small Methods* **2019**, *4*, 4. [[CrossRef](#)]

80. Qin, Y.; Wen, J.; Zheng, L.; Yan, H.; Jiao, L.; Wang, X.; Cai, X.; Wu, Y.; Chen, G.; Chen, L.; et al. Single-Atom-Based Heterojunction Coupling with Ion-Exchange Reaction for Sensitive Photoelectrochemical Immunoassay. *Nano Lett.* **2021**, *21*, 1879–1887. [[CrossRef](#)]
81. You, F.; Zhu, M.; Ding, L.; Xu, Y.; Wang, K. Design and construction of Z-scheme Bi₂S₃/nitrogen-doped graphene quantum dots: Boosted photoelectric conversion efficiency for high-performance photoelectrochemical aptasensing of sulfadimethoxine. *Biosens. Bioelectron.* **2019**, *130*, 230–235. [[CrossRef](#)] [[PubMed](#)]
82. Liu, Q.; Huan, J.; Hao, N.; Qian, J.; Mao, H.; Wang, K. Engineering of Heterojunction-Mediated Bointerface for Photoelectrochemical Aptasensing: Case of Direct Z-Scheme CdTe-Bi₂S₃ Heterojunction with Improved Visible-Light-Driven Photoelectrical Conversion Efficiency. *ACS Appl. Mater. Interfaces* **2017**, *9*, 18369–18376. [[CrossRef](#)] [[PubMed](#)]
83. Cui, L.; Hu, J.; Wang, M.; Diao, X.-K.; Li, C.-C.; Zhang, C.-Y. Mimic Peroxidase- and Bi₂S₃ Nanorod-Based Photoelectrochemical Biosensor for Signal-On Detection of Polynucleotide Kinase. *Anal. Chem.* **2018**, *90*, 11478–11485. [[CrossRef](#)]
84. Li, D.; Xing, G.; Tang, S.; Li, X.; Fan, L.; Li, Y. Ultrathin ZnSe nanowires: One-pot synthesis via a heat-triggered precursor slow releasing route, controllable Mn doping and application in UV and near-visible light detection. *Nanoscale* **2017**, *9*, 15044–15055. [[CrossRef](#)] [[PubMed](#)]
85. Liu, M.; Ding, X.; Yang, Q.; Wang, Y.; Zhao, G.; Yang, N. A pM leveled photoelectrochemical sensor for microcystin-LR based on surface molecularly imprinted TiO₂@CNTs nanostructure. *J. Hazard. Mater.* **2017**, *331*, 309–320. [[CrossRef](#)]
86. Zhang, X.; Yan, T.; Wu, T.; Feng, Y.; Sun, M.; Yan, L.; Du, B.; Wei, Q. Fabrication of hierarchical MIL-68(In)-NH₂/MWCNT/CdS composites for constructing label-free photoelectrochemical tetracycline aptasensor platform. *Biosens. Bioelectron.* **2019**, *135*, 88–94. [[CrossRef](#)] [[PubMed](#)]
87. Lu, Y.; Lu, X.; Gu, S.; Shi, X.-M.; Fan, G.-C. Enhanced two-electrode photoelectrochemical biosensing platform amplified by bilirubin oxidase labelling. *Sens. Actuators B Chem.* **2021**, *343*, 130060. [[CrossRef](#)]
88. Novoselov, K.S.; Geim, A.K.; Morozov, S.V.; Jiang, D.; Zhang, Y.; Dubonos, S.V.; Grigorieva, I.V.; Firsov, A.A. Electric field effect in atomically thin carbon films. *Science* **2004**, *306*, 666–669. [[CrossRef](#)]
89. Meng, Z.; Stolz, R.M.; Mendecki, L.; Mirica, K.A. Electrically-Transduced Chemical Sensors Based on Two-Dimensional Nanomaterials. *Chem. Rev.* **2019**, *119*, 478–598. [[CrossRef](#)]
90. Okoth, O.K.; Yan, K.; Zhang, J. Mo-doped BiVO₄ and graphene nanocomposites with enhanced photoelectrochemical performance for aptasensing of streptomycin. *Carbon* **2017**, *120*, 194–202. [[CrossRef](#)]
91. Ge, L.; Liu, Q.; Jiang, D.; Ding, L.; Wen, Z.; Guo, Y.; Ding, C.; Wang, K. Oxygen vacancy enhanced photoelectrochemical performance of Bi₂MoO₆/B, N co-doped graphene for fabricating lincomycin aptasensor. *Biosens. Bioelectron.* **2019**, *135*, 145–152. [[CrossRef](#)] [[PubMed](#)]
92. Zhao, S.; Zhang, J.; Li, Z.; Zhang, P.; Li, Y.; Liu, G.; Wang, Y.; Yue, Z. Photoelectrochemical determination of hydrogen peroxide using a gold electrode modified with fluorescent gold nanoclusters and graphene oxide. *Microchim. Acta* **2017**, *184*, 677–686. [[CrossRef](#)]
93. Peng, M.; Guan, G.; Deng, H.; Han, B.; Tian, C.; Zhuang, J.; Xu, Y.; Liu, W.; Lin, Z. PCN-224/rGO nanocomposite based photoelectrochemical sensor with intrinsic recognition ability for efficient p-arsanilic acid detection. *Environ. Sci. Nano* **2019**, *6*, 207–215. [[CrossRef](#)]
94. Qian, Y.; Feng, J.; Fan, D.; Zhang, Y.; Kuang, X.; Wang, H.; Wei, Q.; Ju, H. A sandwich-type photoelectrochemical immunosensor for NT-pro BNP detection based on F-Bi₂WO₆/Ag₂S and GO/PDA for signal amplification. *Biosens. Bioelectron.* **2019**, *131*, 299–306. [[CrossRef](#)]
95. Zhou, Q.; Xue, H.; Zhang, Y.; Lv, Y.; Li, H.; Liu, S.; Shen, Y.; Zhang, Y. Metal-Free All-Carbon Nanohybrid for Ultrasensitive Photoelectrochemical Immunosensing of alpha-Fetoprotein. *ACS Sens.* **2018**, *3*, 1385–1391. [[CrossRef](#)]
96. Wang, Y.; Zhang, R.; Zhang, Z.; Cao, J.; Ma, T. Host–Guest Recognition on 2D Graphitic Carbon Nitride for Nanosensing. *Adv. Mater. Interfaces* **2019**, *6*, 6. [[CrossRef](#)]
97. Mazhabi, R.M.; Ge, L.; Jiang, H.; Wang, X. A facile photoelectrochemical sensor for high sensitive ROS and AA detection based on graphitic carbon nitride nanosheets. *Biosens. Bioelectron.* **2018**, *107*, 54–61. [[CrossRef](#)]
98. Yan, P.; Dong, J.; Mo, Z.; Xu, L.; Qian, J.; Xia, J.; Zhang, J.; Li, H. Enhanced photoelectrochemical sensing performance of graphitic carbon nitride by nitrogen vacancies engineering. *Biosens. Bioelectron.* **2020**, *148*, 111802. [[CrossRef](#)] [[PubMed](#)]
99. Peng, B.; Tang, L.; Zeng, G.; Fang, S.; Ouyang, X.; Long, B.; Zhou, Y.; Deng, Y.; Liu, Y.; Wang, J. Self-powered photoelectrochemical aptasensor based on phosphorus doped porous ultrathin g-C₃N₄ nanosheets enhanced by surface plasmon resonance effect. *Biosens. Bioelectron.* **2018**, *121*, 19–26. [[CrossRef](#)]
100. Chen, X.; Zhang, W.; Zhang, L.; Feng, L.; Zhang, C.; Jiang, J.; Wang, H. Turning on the Photoelectrochemical Responses of Cd Probe-Deposited g-C₃N₄ Nanosheets by Nitrogen Plasma Treatment toward a Selective Sensor for H₂S. *ACS Appl. Mater. Interfaces* **2021**, *13*, 2052–2061. [[CrossRef](#)] [[PubMed](#)]
101. Tang, L.; Ouyang, X.; Peng, B.; Zeng, G.; Zhu, Y.; Yu, J.; Feng, C.; Fang, S.; Zhu, X.; Tan, J. Highly sensitive detection of microcystin-LR under visible light using a self-powered photoelectrochemical aptasensor based on a CoO/Au/g-C₃N₄ Z-scheme heterojunction. *Nanoscale* **2019**, *11*, 12198–12209. [[CrossRef](#)]
102. Lv, S.; Li, Y.; Zhang, K.; Lin, Z.; Tang, D. Carbon Dots/g-C₃N₄ Nanoheterostructures-Based Signal-Generation Tags for Photoelectrochemical Immunoassay of Cancer Biomarkers Coupling with Copper Nanoclusters. *ACS Appl. Mater. Interfaces* **2017**, *9*, 38336–38343. [[CrossRef](#)]

103. Zhang, Y.; Xu, R.; Kang, Q.; Zhang, Y.; Wei, Q.; Wang, Y.; Ju, H. Ultrasensitive Photoelectrochemical Biosensing Platform for Detecting N-Terminal Pro-brain Natriuretic Peptide Based on SnO₂/SnS₂/mpg-C₃N₄ Amplified by PbS/SiO₂. *ACS Appl. Mater. Interfaces* **2018**, *10*, 31080–31087. [[CrossRef](#)]
104. Li, P.-P.; Cao, Y.; Mao, C.-J.; Jin, B.-K.; Zhu, J.-J. TiO₂/g-C₃N₄/CdS Nanocomposite-Based Photoelectrochemical Biosensor for Ultrasensitive Evaluation of T4 Polynucleotide Kinase Activity. *Anal. Chem.* **2019**, *91*, 1563–1570. [[CrossRef](#)]
105. Gao, Y.; Zhang, J.; Zhang, X.; Li, J.; Zhang, R.; Song, W. Liposomal Controlled Release Ag-Activated DNzyme Cycle Amplification on a 2D Pyrene COF-Based Photocathode for α -Synuclein Immunosensing. *Anal. Chem.* **2021**, *93*, 8647–8655. [[CrossRef](#)]
106. Jiao, S.; Liu, L.; Wang, J.; Ma, K.; Lv, J. A Novel Biosensor Based on Molybdenum Disulfide (MoS₂) Modified Porous Anodic Aluminum Oxide Nanochannels for Ultrasensitive microRNA-155 Detection. *Small* **2020**, *16*, e2001223. [[CrossRef](#)] [[PubMed](#)]
107. Han, F.; Song, Z.; Nawaz, M.H.; Dai, M.; Han, D.; Han, L.; Fan, Y.; Xu, J.; Han, D.; Niu, L. MoS₂/ZnO-Heterostructures-Based Label-Free, Visible-Light-Excited Photoelectrochemical Sensor for Sensitive and Selective Determination of Synthetic Antioxidant Propyl Gallate. *Anal. Chem.* **2019**, *91*, 10657–10662. [[CrossRef](#)]
108. Lu, M.; Li, B.; Zhang, Y.; Liang, Q.; Li, X.; Xu, S.; Li, Z. Facile synthesis and characterization of a cobalt phthalocyanine sensitized SnIn₄S₈ composites toward enhanced photocatalytic activity. *J. Mater. Sci. Mater. Electron.* **2018**, *29*, 16680–16690. [[CrossRef](#)]
109. Ding, L.; Jiang, D.; Wen, Z.; Xu, Y.; Guo, Y.; Ding, C.; Wang, K. Ultrasensitive and visible light-responsive photoelectrochemical aptasensor for edifenphos based on Zinc phthalocyanine sensitized MoS₂ nanosheets. *Biosens. Bioelectron.* **2020**, *150*, 111867. [[CrossRef](#)] [[PubMed](#)]
110. Hu, D.; Cui, H.; Wang, X.; Luo, F.; Qiu, B.; Cai, W.; Huang, H.; Wang, J.; Lin, Z. Highly Sensitive and Selective Photoelectrochemical Aptasensors for Cancer Biomarkers Based on MoS₂/Au/GaN Photoelectrodes. *Anal. Chem.* **2021**, *93*, 7341–7347. [[CrossRef](#)]
111. Raza, F.; Park, J.H.; Lee, H.-R.; Kim, H.-I.; Jeon, S.-J.; Kim, J.-H. Visible-Light-Driven Oxidative Coupling Reactions of Amines by Photoactive WS₂ Nanosheets. *ACS Catal.* **2016**, *6*, 2754–2759. [[CrossRef](#)]
112. Li, F.; Zhou, Y.; Wang, S.; Yin, H.; Chen, Y.; Luo, H.; Ai, S. One step preparation of CN-WS₂ nanocomposite with enhanced photoactivity and its application for photoelectrochemical detection of 5-formylcytosine in the genomic DNA of maize seedling. *Biosens. Bioelectron.* **2020**, *151*, 111973. [[CrossRef](#)]
113. Wang, Q.; Yin, H.; Zhou, Y.; Wang, J.; Ai, S. Investigation of the inhibited biotoxicity of heavy metals towards 5-formylcytosine in rice by hydrochar based on photoelectrochemical biosensor. *J. Hazard. Mater.* **2021**, *414*, 125293. [[CrossRef](#)] [[PubMed](#)]
114. Li, F.; Yin, H.; Chen, Y.; Wang, S.; Li, J.; Zhang, Y.; Li, C.; Ai, S. Preparation of P-g-C₃N₄-WS₂ nanocomposite and its application in photoelectrochemical detection of 5-formylcytosine. *J. Colloid Interface Sci.* **2020**, *561*, 348–357. [[CrossRef](#)] [[PubMed](#)]
115. Li, F.; Wang, S.; Yin, H.; Chen, Y.; Zhou, Y.; Huang, J.; Ai, S. Photoelectrochemical Biosensor for DNA Formylation Detection in Genomic DNA of Maize Seedlings Based on Black TiO₂-Enhanced Photoactivity of MoS₂/WS₂ Heterojunction. *ACS Sens.* **2020**, *5*, 1092–1101. [[CrossRef](#)]
116. Qing, M.; Chen, S.L.; Han, L.; Yang, Y.Z.; Luo, H.Q.; Li, N.B. Three-dimensional donor-acceptor-type photoactive material/conducting polyaniline hydrogel complex for sensitive photocathodic enzymatic bioanalysis. *Biosens. Bioelectron.* **2020**, *158*, 112179. [[CrossRef](#)]
117. Zhu, Y.-C.; Liu, Y.-L.; Xu, Y.-T.; Ruan, Y.-F.; Fan, G.-C.; Zhao, W.-W.; Xu, J.-J.; Chen, H.-Y. Three-Dimensional TiO₂@Cu₂O@Nickel Foam Electrodes: Design, Characterization, and Validation of O₂-Independent Photocathodic Enzymatic Bioanalysis. *ACS Appl. Mater. Interfaces* **2019**, *11*, 25702–25707. [[CrossRef](#)]
118. Ge, L.; Li, H.; Du, X.; Zhu, M.; Chen, W.; Shi, T.; Hao, N.; Liu, Q.; Wang, K. Facile one-pot synthesis of visible light-responsive BiPO₄/nitrogen doped graphene hydrogel for fabricating label-free photoelectrochemical tetracycline aptasensor. *Biosens. Bioelectron.* **2018**, *111*, 131–137. [[CrossRef](#)] [[PubMed](#)]
119. Liu, X.; Liu, P.; Tang, Y.; Yang, L.; Li, L.; Qi, Z.; Li, D.; Wong, D.K. A photoelectrochemical aptasensor based on a 3D flower-like TiO₂-MoS₂-gold nanoparticle heterostructure for detection of kanamycin. *Biosens. Bioelectron.* **2018**, *112*, 193–201. [[CrossRef](#)]
120. Wang, S.; Wang, F.; Fu, C.; Sun, Y.; Zhao, J.; Li, N.; Liu, Y.; Ge, S.; Yu, J. AgInSe₂-Sensitized ZnO Nanoflower Wide-Spectrum Response Photoelectrochemical/Visual Sensing Platform via Au@Nanorod-Anchored CeO₂ Octahedron Regulated Signal. *Anal. Chem.* **2020**, *92*, 7604–7611. [[CrossRef](#)]
121. Jalali, M.; Moakhar, R.S.; Abdelfattah, T.; Filine, E.; Mahshid, S.S.; Mahshid, S. Nanopattern-Assisted Direct Growth of Peony-like 3D MoS₂/Au Composite for Nonenzymatic Photoelectrochemical Sensing. *ACS Appl. Mater. Interfaces* **2020**, *12*, 7411–7422. [[CrossRef](#)] [[PubMed](#)]
122. Feng, J.; Li, F.; Li, X.; Wang, Y.; Fan, D.; Du, B.; Li, Y.; Wei, Q. Label-free photoelectrochemical immunosensor for NT-proBNP detection based on La-CdS/3D ZnIn₂S₄/Au@ZnO sensitization structure. *Biosens. Bioelectron.* **2018**, *117*, 773–780. [[CrossRef](#)] [[PubMed](#)]
123. Dong, Y.; Xu, C.; Zhang, L. Construction of 3D Bi/ZnSnO₃ hollow microspheres for label-free highly selective photoelectrochemical recognition of norepinephrine. *Nanoscale* **2021**, *13*, 9270–9279. [[CrossRef](#)] [[PubMed](#)]
124. Hao, N.; Hua, R.; Chen, S.; Zhang, Y.; Zhou, Z.; Qian, J.; Liu, Q.; Wang, K. Multiple signal-amplification via Ag and TiO₂ decorated 3D nitrogen doped graphene hydrogel for fabricating sensitive label-free photoelectrochemical thrombin aptasensor. *Biosens. Bioelectron.* **2018**, *101*, 14–20. [[CrossRef](#)]
125. Li, X.; Yuan, Y.; Pan, X.; Zhang, L.; Gong, J. Boosted photoelectrochemical immunosensing of metronidazole in tablet using coral-like g-C₃N₄ nanoarchitectures. *Biosens. Bioelectron.* **2019**, *123*, 7–13. [[CrossRef](#)]

126. Lan, F.; Liang, L.; Zhang, Y.; Li, L.; Ren, N.; Yan, M.; Ge, S.; Yu, J. Internal Light Source-Driven Photoelectrochemical 3D-rGO/Cellulose Device Based on Cascade DNA Amplification Strategy Integrating Target Analog Chain and DNA Mimic Enzyme. *ACS Appl. Mater. Interfaces* **2017**, *9*, 37839–37847. [[CrossRef](#)]
127. Ye, H.; Yang, K.; Tao, J.; Liu, Y.; Zhang, Q.; Habibi, S.; Nie, Z.; Xia, X. An Enzyme-Free Signal Amplification Technique for Ultrasensitive Colorimetric Assay of Disease Biomarkers. *ACS Nano* **2017**, *11*, 2052–2059. [[CrossRef](#)] [[PubMed](#)]
128. Lou, Z.; Zhao, S.; Wang, Q.; Wei, H. N-Doped Carbon As Peroxidase-Like Nanozymes for Total Antioxidant Capacity Assay. *Anal. Chem.* **2019**, *91*, 15267–15274. [[CrossRef](#)]
129. Vázquez-González, M.; Liao, W.-C.; Cazelles, R.; Wang, S.; Yu, X.; Gutkin, V.; Willner, I. Mimicking Horseradish Peroxidase Functions Using Cu²⁺-Modified Carbon Nitride Nanoparticles or Cu²⁺-Modified Carbon Dots as Heterogeneous Catalysts. *ACS Nano* **2017**, *11*, 3247–3253. [[CrossRef](#)]
130. Chen, Y.; Yuchi, Q.; Li, T.; Yang, G.; Miao, J.; Huang, C.; Liu, J.; Li, A.; Qin, Y.; Zhang, L. Precise engineering of ultra-thin Fe₂O₃ decorated Pt-based nanozymes via atomic layer deposition to switch off undesired activity for enhanced sensing performance. *Sens. Actuators B Chem.* **2020**, *305*, 127436. [[CrossRef](#)]
131. Huang, D.; Wang, L.; Zhan, Y.; Zou, L.; Ye, B. Photoelectrochemical biosensor for CEA detection based on SnS₂-GR with multiple quenching effects of Au@CuS-GR. *Biosens. Bioelectron.* **2019**, *140*, 111358. [[CrossRef](#)]
132. Kong, W.; Guo, X.; Jing, M.; Qu, F.; Lu, L. Highly sensitive photoelectrochemical detection of bleomycin based on Au/WS₂ nanorod array as signal matrix and Ag/ZnMOF nanozyme as multifunctional amplifier. *Biosens. Bioelectron.* **2020**, *150*, 111875. [[CrossRef](#)]
133. Li, W.; Fan, G.-C.; Gao, F.; Cui, Y.; Wang, W.; Luo, X. High-activity Fe₃O₄ nanozyme as signal amplifier: A simple, low-cost but efficient strategy for ultrasensitive photoelectrochemical immunoassay. *Biosens. Bioelectron.* **2019**, *127*, 64–71. [[CrossRef](#)]
134. Zhu, X.; Gao, L.; Tang, L.; Peng, B.; Huang, H.; Wang, J.; Yu, J.; Ouyang, X.; Tan, J. Ultrathin PtNi nanozyme based self-powered photoelectrochemical aptasensor for ultrasensitive chloramphenicol detection. *Biosens. Bioelectron.* **2019**, *146*, 111756. [[CrossRef](#)] [[PubMed](#)]
135. Li, R.; Zhang, Y.; Tu, W.; Dai, Z. Photoelectrochemical Bioanalysis Platform for Cells Monitoring Based on Dual Signal Amplification Using in Situ Generation of Electron Acceptor Coupled with Heterojunction. *ACS Appl. Mater. Interfaces* **2017**, *9*, 22289–22297. [[CrossRef](#)] [[PubMed](#)]
136. Peng, H.; Newbigging, A.M.; Wang, Z.; Tao, J.; Deng, W.; Le, X.C.; Zhang, H. DNAzyme-Mediated Assays for Amplified Detection of Nucleic Acids and Proteins. *Anal. Chem.* **2017**, *90*, 190–207. [[CrossRef](#)] [[PubMed](#)]
137. Gong, L.; Zhao, Z.; Lv, Y.-F.; Huan, S.-Y.; Fu, T.; Zhang, X.-B.; Shen, G.-L.; Yu, R.-Q. DNAzyme-based biosensors and nanodevices. *Chem. Commun.* **2015**, *51*, 979–995. [[CrossRef](#)]
138. Meng, L.; Liu, M.; Xiao, K.; Zhang, X.; Du, C.; Chen, J. Sensitive photoelectrochemical assay of Pb²⁺ based on DNAzyme-induced disassembly of the “Z-scheme” TiO₂/Au/CdS QDs system. *Chem. Commun.* **2020**, *56*, 8261–8264. [[CrossRef](#)]
139. Yan, K.; Ji, W.; Zhu, Y.; Chen, F.; Zhang, J. Photofuel cell coupling with redox cycling as a highly sensitive and selective self-powered sensing platform for the detection of tyrosinase activity. *Chem. Commun.* **2019**, *55*, 12040–12043. [[CrossRef](#)]
140. Hun, X.; Meng, Y. Electron Acceptors Co-Regulated Self-Powered Photoelectrochemical Strategy and Its Application for Circulating Tumor Nucleic Acid Detection Coupled with Recombinase Polymerase Amplification. *Anal. Chem.* **2020**, *92*, 11771–11778. [[CrossRef](#)]
141. Peng, B.; Zhang, Z.; Tang, L.; Ouyang, X.; Zhu, X.; Chen, L.; Fan, X.; Zhou, Z.; Wang, J. Self-Powered Photoelectrochemical Aptasensor for Oxytetracycline Cathodic Detection Based on a Dual Z-Scheme WO₃/g-C₃N₄/MnO₂ Photoanode. *Anal. Chem.* **2021**, *93*, 9129–9138. [[CrossRef](#)]
142. Wang, J.; Zhang, S.; Dai, H.; Zheng, H.; Hong, Z.; Lin, Y. Dual-readout immunosensor constructed based on brilliant photoelectrochemical and photothermal effect of polymer dots for sensitive detection of sialic acid. *Biosens. Bioelectron.* **2019**, *142*, 111567. [[CrossRef](#)]
143. Liu, M.; Chen, G.; Qin, Y.; Li, J.; Hu, L.; Gu, W.; Zhu, C. Proton-Regulated Catalytic Activity of Nanozymes for Dual-Modal Bioassay of Urease Activity. *Anal. Chem.* **2021**, *93*, 9897–9903. [[CrossRef](#)] [[PubMed](#)]
144. Ge, J.; Zhao, Y.; Gao, X.; Li, H.; Jie, G. Versatile Electrochemiluminescence and Photoelectrochemical Detection of Glutathione Using Mn²⁺ Substitute Target by DNA-Walker-Induced Allosteric Switch and Signal Amplification. *Anal. Chem.* **2019**, *91*, 14117–14124. [[CrossRef](#)] [[PubMed](#)]
145. Han, Q.; Zhao, X.; Na, N.; Ouyang, J. Integrating Near-Infrared Visual Fluorescence with a Photoelectrochemical Sensing System for Dual Readout Detection of Biomolecules. *Anal. Chem.* **2021**, *93*, 3486–3492. [[CrossRef](#)] [[PubMed](#)]
146. Wang, Y.; Zhang, L.; Kong, Q.; Ge, S.; Yu, J. Time-resolution addressable photoelectrochemical strategy based on hollow-channel paper analytical devices. *Biosens. Bioelectron.* **2018**, *120*, 64–70. [[CrossRef](#)]
147. Gai, P.; Kong, X.; Zhang, S.; Song, P.; Li, F. Photo-driven self-powered biosensor for ultrasensitive microRNA detection via DNA conformation-controlled co-sensitization behavior. *Chem. Commun.* **2020**, *56*, 7116–7119. [[CrossRef](#)]
148. Yu, Z.; Gong, H.; Li, Y.; Xu, J.; Zhang, J.; Zeng, Y.; Liu, X.; Tang, D. Chemiluminescence-Derived Self-Powered Photoelectrochemical Immunoassay for Detecting a Low-Abundance Disease-Related Protein. *Anal. Chem.* **2021**, *93*, 13389–13397. [[CrossRef](#)] [[PubMed](#)]

149. Lu, M.-J.; Chen, F.-Z.; Hu, J.; Zhou, H.; Chen, G.; Yu, X.-D.; Ban, R.; Lin, P.; Zhao, W.-W. Regulating Light-Sensitive Gate of Organic Photoelectrochemical Transistor toward Sensitive Biodetection at Zero Gate Bias. *Small Struct.* **2021**, *2*, 2100087. [[CrossRef](#)]
150. Ruan, Y.; Chen, F.; Xu, Y.; Zhang, T.; Yu, S.; Zhao, W.; Jiang, D.; Chen, H.; Xu, J. An Integrated Photoelectrochemical Nanotool for Intracellular Drug Delivery and Evaluation of Treatment Effect. *Angew. Chem. Int. Ed.* **2021**, *60*, 25762–25765. [[CrossRef](#)]